ACS OMEGA

Open Access

http://pubs.acs.org/journal/acsodf

Article

4″-Alkyl EGCG Derivatives Induce Cytoprotective Autophagy Response by Inhibiting EGFR in Glioblastoma Cells

Satyam Singh, Priya Ghosh,[‖] Rajarshi Roy,[‖] Ananyaashree Behera, Revathy Sahadevan, Parimal Kar, Sushabhan Sadhukhan,* and Avinash Sonawane*

Cite This: *ACS Omega* 2024, 9, 2286−2301

Read Online

ACCESS | Metrics & More | Article Recommendations | Supporting Information

ABSTRACT: Epidermal growth factor receptor (EGFR)-targeted therapy has been proven vital in the last two decades for the treatment of multiple cancer types, including nonsmall cell lung cancer, glioblastoma, breast cancer and head and neck squamous cell carcinoma. Unfortunately, the majority of approved EGFR inhibitors fall into the drug resistance category because of continuous mutations and acquired resistance. Recently, autophagy has surfaced as one of the emerging underlying mechanisms behind resistance to EGFR-tyrosine kinase inhibitors (TKIs). Previously, we developed a series of 4″-alkyl EGCG (4″-C_n EGCG, n = 6, 8, 10, 12, 14, 16, and 18) derivatives with enhanced anticancer effects and stability. Therefore, the current study hypothesized that 4″-alkyl EGCG might induce cytoprotective autophagy upon EGFR inhibition, and inhibition of autophagy may lead to improved cytotoxicity. In this study, we have observed growth inhibition and caspase-3-dependent apoptosis in 4″-alkyl EGCG derivative-treated glioblastoma cells (U87-MG). We also confirmed that 4″-alkyl EGCG could inhibit EGFR in the cells, as well as mutant L858R/T790M EGFR, through an in vitro kinase assay. Furthermore, we have found that EGFR inhibition with 4″-alkyl EGCG induces cytoprotective autophagic responses, accompanied by the blockage of the AKT/mTOR signaling pathway. In addition, cytotoxicity caused by 4″-C_{10} EGCG, 4″-C_{12} EGCG, and 4″-C_{14} EGCG was significantly increased after the inhibition of autophagy by the pharmacological inhibitor chloroquine. These findings enhance our understanding of the autophagic response toward EGFR inhibitors in glioblastoma cells and suggest a potent combinatorial strategy to increase the therapeutic effectiveness of EGFR-TKIs.

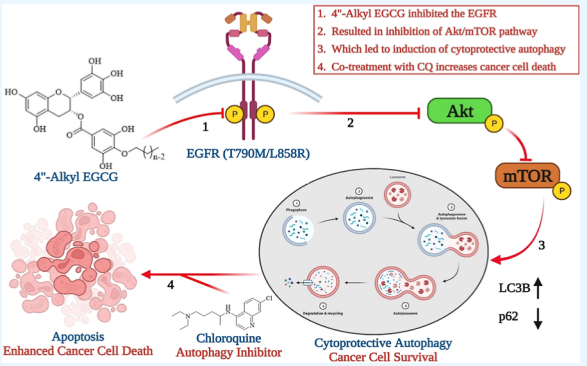

1. INTRODUCTION

Glioblastoma (GBM) is a highly invasive primary malignant brain cancer of the central nervous system and accounts for 60% of brain cancer cases in adults.[1−3] Kinases have been associated with the progression of GBM and are considered potential therapeutic targets.[4−6] Protein kinases are enzymes that play a crucial role in cell signaling pathways, regulating various cellular processes, including growth, proliferation, and survival.[7] Remarkable advancements have been made in the past two decades for the development of potent and specific small-molecule kinase inhibitors, and kinase inhibitors hold significant potential as precise therapeutic agents for cancer treatment.[5,8] These kinase inhibitors includes, but are not limited to epidermal growth factor receptor (EGFR) (gefitinib,[9] afatinib,[10] and osimertinib[11]), human epidermal growth factor 2 (HER2/ERBB2) (lapatinib,[12] neratinib,[5] and tucatinib[5]), vascular endothelial growth factor receptor (VEGFR) (tivozanib and lenvatinib),[13] fibroblast growth factor receptor (erdafitinib),[14] Abelson (ABL) tyrosine kinase (imatinib, dasatinib, and nilotinib),[5,15] Bruton's tyrosine kinase (ibrutinib, acalabrutinib, and zanubrutinib),[16] cyclin/cyclin-dependent kinase 4 and 6 (CDK4/CDK6) (palbociclib and ribociclib),[17] etc. Kinase inhibitors are widely being utilized in clinical settings as promising cancer therapeutics. Among them, EGFR tyrosine kinase is one of the key targets for antitumor therapeutic agents[18] and is commonly found upregulated in several types of cancer, including GBM, lung cancer, breast cancer, and colorectal cancer;[4,19] therefore, EGFR is being considered a promising central druggable target.[8] The autophosphorylation of EGFR leads to the activation of downstream signaling pathways, such as Ras/MAPK/ERK and PI3K/Akt/mTOR, which are crucial for cell differentiation, survival, migration, and disease regulation, including cancer.[20] Therefore, blocking EGFR with tyrosine kinase inhibitors (TKIs) has become an important strategy for cancer therapy.[21] EGFR-TKIs such as gefitinib, afatinib, and osimertinib have been developed to effectively inhibit EGFR and have shown promising clinical

Received: August 17, 2023
Revised: November 8, 2023
Accepted: November 16, 2023
Published: January 3, 2024

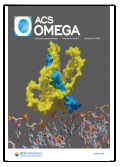

outcomes in EGFR-active cancer patients.[22,23] However, the development of natural and acquired resistance to EGFR-TKIs is a major challenge for cancer treatment,[8,23,24] and currently, major efforts are being made to develop a new class of EGFR blockers to overcome EGFR-TKI-mediated drug resistance.

Various studies have reported that EGFR regulates macroautophagy (hereafter referred to as autophagy),[25,26] which is an important lysosomal degradation pathway known for the regulation of cellular homeostasis and involved in both cancer progression and suppression.[27] By enabling the survival of cancer cells during unfavorable conditions, autophagy prevents tumor cells from undergoing apoptosis or necrosis induced by several anticancer agents and acts as an alternative mode of drug resistance.[28] Notably, the downstream signaling pathway of EGFR, PI3K/Akt/mTOR, negatively regulates autophagy, indicating an important link between EGFR inhibition and autophagy.[29,30]

(−)-Epigallocatechin-3-*O*-gallate (EGCG), a major green tea polyphenol and therapeutically active compound known to elicit health-beneficial activities against diseases, including cancer.[31−34] EGCG exhibits its anticancer activity by regulating various signaling pathways associated with cancer progression.[35] However, low bioavailability, poor stability,[31,36] and less membrane permeability minimize the use of EGCG as a therapeutic agent.[37,38] To overcome these shortcomings, various structural derivatizations of EGCG have been carried out to enhance its biological activities.[31] In this context, monoalkylated EGCG (C18-EGCG) was already synthesized in 2020 by Minnelli et al. to improve the lipophilicity and biological activity of EGCG.[39] Previously, we also designed and synthesized a series of 4″-alkyl derivatives (4″-C_n EGCG) of EGCG, where 4″-C_{14} EGCG effectively inhibited the EGF-induced phosphorylation of EGFR in A431 cells.[40] In recent times, cytoprotective autophagy has emerged as one of the resistance mechanisms to EGFR-TKIs.[41] This prompted us to investigate whether inhibition of EGFR by 4″-alkyl EGCG derivatives also leads to the induction of cytoprotective autophagy in GBM. Hence, we investigated the inhibitory effect of 4″-alkyl EGCG derivatives along with the parent compound EGCG against EGFR and the induction of cytoprotective autophagy upon EGFR inhibition in the GBM cell line, U87-MG. In this study, we checked the inhibitory profiles of 4″-alkyl EGCG derivatives and EGCG against the double mutant EGFR (T790M/L858R) through Western blot analysis, in vitro kinase assay, and MD simulation studies. We observed that upon EGFR inhibition, 4″-alkyl EGCG initiated the autophagic response in U87-MG cells. After, the blockage of autophagy sensitizes U87-MG against 4″-alkyl EGCG treatment, suggesting that during this process, autophagy played a survival role.

2. MATERIAL AND METHODS

2.1. Cell Culture and Materials. U87-MG cells were purchased from the National Center for Cell Science (Pune, India). U87-MG cells were grown in Dulbecco's modified Eagle medium (DMEM; Gibco), supplemented with 10% fetal bovine serum (FBS; Gibco), at 37 °C, with 5% CO_2 and 90% humidity.

All the 4″-alkyl EGCG (4″-C_n EGCG, n = 6, 8, 10, 12, 14, 16, and 18 carbon chain length) derivatives were synthesized and characterized as per our previously published report.[40] Briefly, the 4″-alkyl EGCG derivatives were obtained from a 2 h controlled single step reaction between EGCG (0.65 mmol, 1 equivalent) and 1-bromoalkanes (3.25 mmol, 5 equivalent) in the presence of a weak base, anhydrous sodium acetate (NaOAc) (1.94 mmol, equivalent), in the solvent *N*,*N*′-dimethyl formamide (DMF) (3 mL) at 85 °C. The progress of the reaction was monitored using thin-layer chromatography. The reaction was stopped by the addition of water after 2 h, and the crude product was extracted using ethyl acetate (three times), followed by solvent evaporation using a rotary evaporator. The pure product with high purity (>98%) and yield (>50%) was obtained from silica gel column chromatography with the crude extract. Finally, the structure of the compounds was characterized and confirmed by various analytical techniques (ESI-LC-MS, FT-IR, ^{1}H NMR, ^{13}C NMR, and HMBC NMR).[40] EGCG was purchased from Carbosynth Ltd., UK, and chloroquine (CQ) and gefitinib were purchased from Sigma-Aldrich.

All of the compounds were dissolved in dimethyl sulfoxide (DMSO; Sigma-Aldrich). Hoechst 33342 and propidium iodide (PI) were purchased from Himedia. Anti-pEGFR (Y1068; no. 3777S), pAkt (no. 4060S), Akt (no. 4691S), *p*-mTOR (no. 5536S), mTOR (no. 2983), LC3B (no. 83506S), SQSTM1/p62 (no. 8025S), BCL_{XL} (no. 2764), Cleaved caspase-3 (no. 9664S), and antibodies were purchased from Cell Signaling Technology. Anti-EGFR (sc-373746) and β-actin (sc-47778) were purchased from Santa-Cruz Biotechnology.

2.2. Antiproliferative Assay. Cell proliferation was assessed by using a standard CCK-8 assay (Dojindo Molecular Technologies, Inc., Kumamoto, Japan). Briefly, 1×10^4 cells/well were seeded in 96-well plates and treated with various concentrations of 4″-alkyl EGCG derivatives, EGCG and Gefitinib, for 24 h. Next, 10 μL of the CCK-8 reagent was added to each well, and the 96-well plates were incubated at 37 °C for 2 h. Then, the absorbance was measured at 450 nm by using a microplate reader (Synergy H1 microplate reader, Biotek).

2.3. Fluorescence Staining. To assess the apoptotic cells upon 4″-alkyl EGCG derivatives treated U87-MG cells, Hoechst 33342/PI double staining was carried out. Briefly, 1×10^5 cells (U87-MG) were seeded on glass coverslips in 12-well plates for 24 h and then treated with 4″-alkyl EGCG derivatives, EGCG at 50 μM and Gefitinib at 5 μM for the next 24 h. Then, cells were washed thrice with 1× phosphate buffer saline (PBS), followed by cells being fixed with 4% paraformaldehyde and stained with PI (15 μg mL^{-1}) and Hoechst 33342 (10 μg mL^{-1}) for 30 min or with 20 μg/mL Acridine Orange (Sigma) at 37 °C for 20 min. Cells were observed under a fluorescence microscope (Olympus IX83, Tokyo, Japan).

2.4. Flow Cytometry. Cellular apoptosis was measured by flow cytometry analysis. The experiment was carried out according to the manufacturer's protocol (Annexin V-FITC Apoptosis Detection Kit, Sigma). 4×10^5 cells were seeded in six-well plates and then treated with 50 μM of 4″-alkyl EGCG derivatives, EGCG and 5 μM Gefitinib, for 24 h. After the treatment, cells were harvested, washed three times with 1X PBS, and resuspended in binding buffer. Then, the cells were stained with Annexin-V-FITC and PI for 15 min at room temperature. Apoptosis was quantified using flow cytometry (BD FACS Aria III) and analyzed by FlowJo software.

2.5. Western Blot. The Western blot experiment was carried out as per the previously published reports from our group.[40,42,43] Briefly, after washing three times with 1X cold PBS, cells were lysed in RIPA buffer (1 M Tris pH 7.4, 2 M NaCl, 0.1 M EDTA, 1 M PMSF100 mM DTT, 1 mM sodium orthovanadate, Triton-X-100, glycerol and protease inhibitor cocktail, and phosphatase inhibitor cocktail) and collected. After

https://doi.org/10.1021/acsomega.3c06110
ACS Omega 2024, 9, 2286−2301

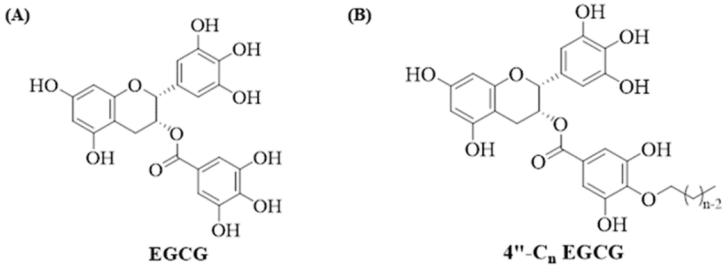

(C)

Compound name	IC_{50} (μM)
	U87-MG
4"-C_6 EGCG	63.36 ± 0.05
4"-C_8 EGCG	40.79 ± 0.13
4"-C_{10} EGCG	107.8 ± 0.03
4"-C_{12} EGCG	74.56 ± 0.01
4"-C_{14} EGCG	**26.07 ± 0.08**
4"-C_{16} EGCG	82.16 ± 0.06
4"-C_{18} EGCG	117.3 ± 0.02
EGCG	61.36 ± 0.06
Gefitinib	6.49 ± 0.10

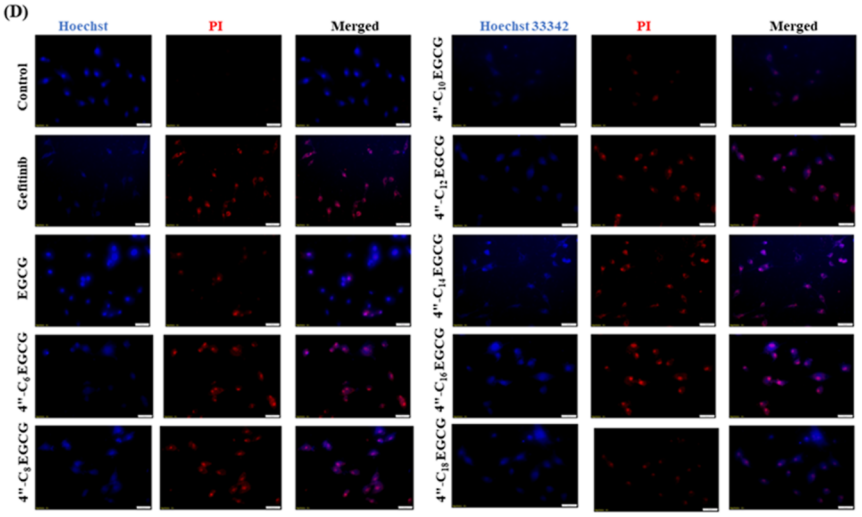

Figure 1. 4″-alkyl EGCG derivatives induce cytotoxicity in U87-MG cells. (A and B) Structure of EGCG and 4″-alkyl EGCG (4″-C_n EGCG), where n = 6, 8, 10, 12, 14, 16, and 18. (C) Antiproliferative effects of 4″-alkyl EGCG derivatives against the U87-MG cell line measured by using the CCK-8 assay after 24 h of treatment. The IC_{50} values are expressed as (mean ± SEM). (D) U87-MG cells treated with 4″-alkyl EGCG (corresponding concentration of 50 μM, except Gefitinib, which was 5 μM) at 24 h and stained with Hoechst 33342/PI dye. Scale bar is 50 μM (original magnification 20×).

centrifugation at 13,000 rpm for 20 min at 4 °C, the protein content was determined using a Bradford assay. An equal amount of protein was loaded for gel electrophoresis at 50 mA, followed by transfer onto nitrocellulose membranes (120 min, 100 V) (Bio-Rad). Membranes were then blocked using 5% skimmed milk for 2 h at room temperature and then incubated overnight at 4 °C with primary antibodies on a rocker. Subsequently, the membranes were washed three times with 1× PBST and incubated with horseradish peroxidase-conjugated antirabbit/antimouse IgG secondary antibodies for 2 h and visualized using the Fusion Solo S chemidoc system (Vilber). Protein band intensities were quantified using Image J software (NIH) with respect to β-actin.

2.6. In Vitro Kinase Assay. For WT-EGFR and T790M/L858R EGFR inhibitory activity, the Z′-LYTE Kinase Assay Kit—tyrosine 4 peptide, procured from Invitrogen Bioservices India Pvt. Ltd. (PV3193), was used, and the assays were carried out according to the protocol provided by the manufacturers. The kinases used, WT EGFR (14-531) and T790M/L858R EGFR (14-721), were purchased from the EMD Millipore Corporation, Massachusetts, USA. The 2× EGFR (WT and T790M/L858R)/ Z′-LYTE Tyr 4 peptide mixture was prepared in 50 mM HEPES pH 6.5, 0.01% BRIJ-35, 10 mM $MgCl_2$, and 1 mM EGTA. The final 10 μL Kinase Reaction consists of 5 μL of kinase (25 ng of WT EGFR and 40 ng of T790M/L858R EGFR) and 2 μM Tyr 4, 2.5 μL of 10 μM ATP, and 2.5 μL of various concentrations (1 nM to 5 μM) of EGCG and 4″-alkyl EGCG

https://doi.org/10.1021/acsomega.3c06110
ACS Omega 2024, 9, 2286−2301

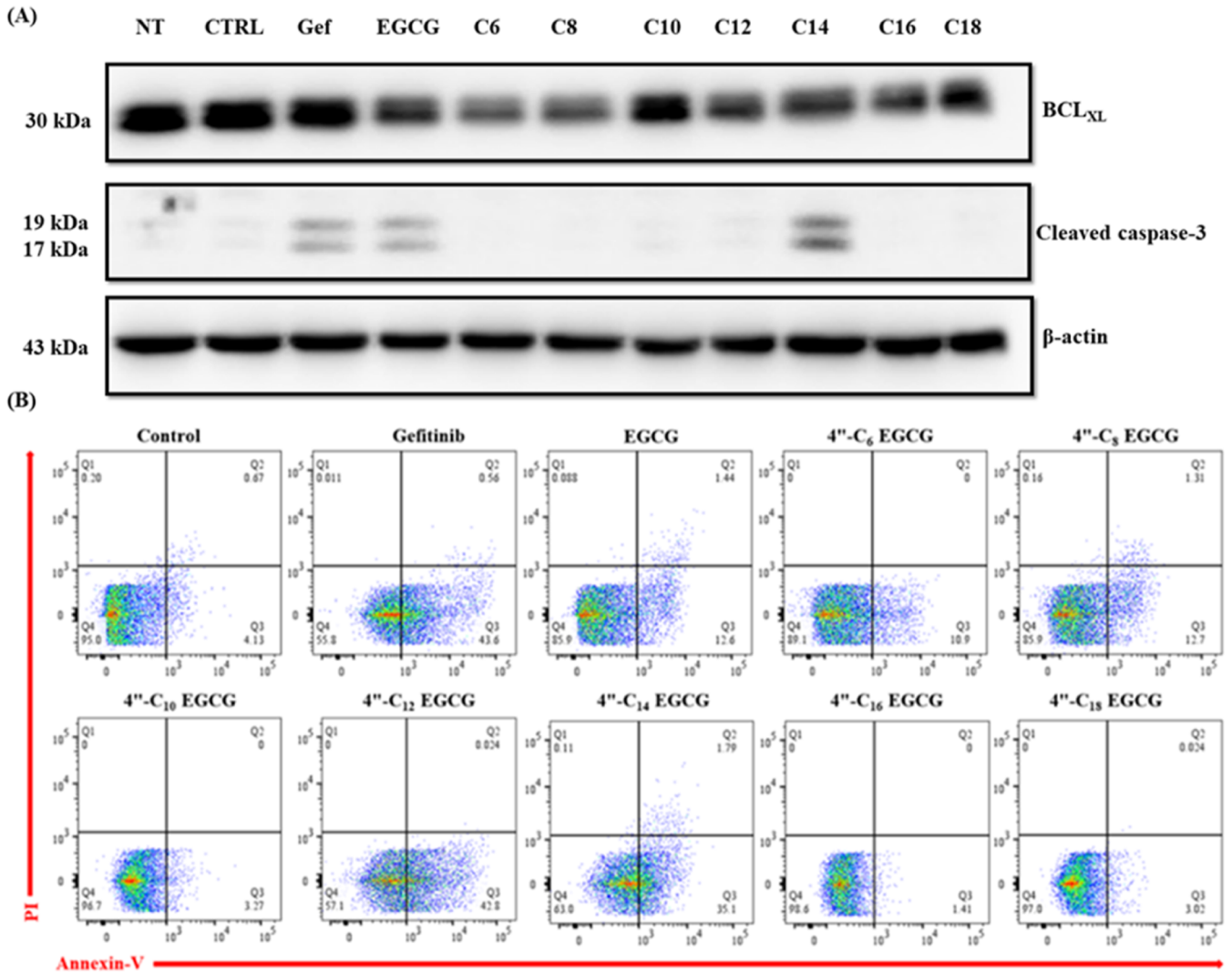

Figure 2. 4″-Alkyl EGCG derivatives induce apoptosis. (A) U87-MG cells were incubated with 5 μM Gefitinib and 50 μM of EGCG and 4″-alkyl EGCG derivatives for 24 h; then, the expression level of the antiapoptotic marker BCL$_{XL}$ and cleaved caspase-3 was measured by Western blot analysis. (B) Flow cytometry analysis was carried out to detect cell apoptosis after 24 h treatment with 5 μM Gefitinib and 50 μM of EGCG and 4″-alkyl EGCG derivatives. Annexin-V-positive cells were defined as apoptotic cells.

(4″-C$_{10}$ EGCG, 4″-C$_{12}$ EGCG, and 4″-C$_{14}$ EGCG) dissolved in DMSO. After 1 h of kinase reaction incubation, 5 μL of development reagent B was added, and the 15 μL development reaction was continued for 1 h at room temperature in the dark. Next, the kinase reaction was stopped by adding 5 μL of stop reagent. In the last, the fluorescence signals were immediately measured by using the fluorescence microplate reader, Synergy H1, Biotek, at 445 and 520 nm for both donor and acceptor emission, respectively, to calculate the emission ratio.

2.7. Molecular Docking. To investigate the binding interaction of the 4″-alkyl EGCG with WT-EGFR (PDB ID: 4I23) and T790M/L858R EGFR (PDB ID: 5EDP), a molecular docking study was conducted using the GLIDE module of the Schrodinger software suite.[44,45] Prior to the docking run, we utilized MODELLAR[46] to reconstruct the missing regions of the EGFR crystal, specifically the missing loop close to the binding pocket, encompassing residues 720−724 and 747−750 for the WT-EGFR, and residues 720−724 and 859−875 for the T790M/L858R mutant EGFR. The protein preparation wizard of Maestro was used to perform protein preparation and protein refinement before docking. After preparation, water molecules of the crystal structure were removed, and the missing hydrogen atoms were added to the structure. The OPLS3 forcefield was used to minimize the complex structures to remove any steric clashes.[47] The binding site of the cocrystallized ligand, dacomitinib, was used to create a receptor grid, and the docking was performed by using the extra precision algorithm of GLIDE (GLIDE-XP) to achieve higher accuracy. A similar docking protocol was also followed for the mutant EGFR (T790M/L858R) crystal structure (PDB ID: 5EDP). The best binding pose was identified by estimating GScore, which includes key interactions such as hydrophobic interactions, hydrogen bond interactions, stacking interactions, etc. Furthermore, the coordinate of the best pose for each ligand complex was used as the initial input for conventional molecular dynamics (cMD).

2.8. MD Simulation. The thermodynamic stability and atomistic details of the interaction between ligands and EGFR kinase were assessed using cMD by the pmemd.cuda module of AMBER18. The ff14SB[48] and GAFF2[49] forcefields were used for protein and ligand, respectively, for each complex. All synthesized ligand parameters were estimated using the antechamber module of the AMBER18 suite.[50] The initial

https://doi.org/10.1021/acsomega.3c06110
ACS Omega 2024, 9, 2286−2301

structures were neutralized and solvated with adequate Na^+/Cl^- ions in a TIP3P[51] water box with a buffering distance of 10 Å from all sides of the systems. A two-stage geometric optimization was performed upon the positions of solvent molecules only, followed by an unrestrained minimization of all of the atoms. This was followed by a stepwise temperature increment from 0 to 300 K, and the SHAKE algorithm was used to restrain all bonds involving hydrogen atoms.[52] The long-range electrostatic interactions were modeled using the particle mesh Ewald method (PME)[53] method with a 10 Å cutoff for all nonbonded interactions. The system's temperature and pressure were kept constant at around 300 K and 1 bar using a Langevin thermostat and Berendsen barostat, respectively.[54,55] A detailed simulation protocol was discussed in our previous work.[56−59] Finally, 2 × 400 ns long production MD runs were performed for all complexes under the *NPT* ensemble with a 2 fs time step, and the trajectories were analyzed using the Cpptraj module of AmberTools19.[60]

2.9. Binding Free Energy Calculation. The molecular mechanics Poisson−Boltzmann surface area (MMPBSA) scheme was used to estimate the binding free energy of all protein−ligand complexes. This method is widely used for estimating the binding free energy of various biomolecular complexes.[61−63] Frames were used from the last 200 ns of the trajectories, and the binding energy was estimated using the following equation.[64]

$$\Delta G_{bind} = \Delta H - T\Delta S \approx \Delta E_{internal} + \Delta G_{solv} - T\Delta S \quad (1)$$

The total binding free energy (ΔG_{bind}) comprises internal energy ($\Delta E_{internal}$), desolvation-free energy (ΔG_{solv}), and configurational entropy ($T\Delta S$). Due to the high computational cost, the estimation of entropy was neglected.

2.10. Statistical Analysis. Statistical analysis was performed using GraphPad Prism 6.0, and the data are presented as the mean ± SEM. A one-way ANOVA test followed by Dunnett's multiple comparison test was applied to test the difference between the control and treated groups. A level of $*p < 0.1$ was considered significant, and $**p < 0.05$, $***p < 0.01$, or $****p < 0.001$ was considered extremely significant. A level of $p > 0.1$ (ns) was considered not significant.

3. RESULTS

3.1. 4″-Alkyl EGCG Derivatives Inhibit Growth of GBM Cells. 4″-Alkyl EGCG derivatives (0−200 μM) were evaluated for their anticancer activities against human GBM cell line U87-MG after 24 h of treatment using the CCK-8 assay. The IC_{50} for each EGCG derivative in U87-MG cells was calculated, and the results are summarized in Figure 1C. As evident from Figure 1C, the best IC_{50} values among the derivatives were observed for 4″-C_{14} EGCG, 4″-C_8 EGCG, and 4″-C_6 EGCG, with IC_{50} values of 26.07 ± 0.08, 40.79 ± 0.13 μM, and 63.36 ± 0.05 μM, respectively. EGCG (reference compound) and first-generation EGFR TKI Gefitinib, which was taken as the positive control, exhibited IC_{50} values of 61.36 ± 0.05 and 6.49 ± 0.10 μM, respectively, in U87-MG.

Hoechst 33342/PI dual staining was carried out to assess the apoptotic cells upon 4″-alkyl EGCG derivative treatment via fluorescence microscopy (Figure 1D). Initially, we selected a 25 μM concentration for all the derivatives to carry out the Hoechst 33342/PI double staining, and we observed that except for 4″-C_{14} EGCG, none of the derivatives were promising to induce cell death in U87-MG (data not shown). Thus, we selected a 50 μM concentration for further experiments. The obtained results are shown in Figure 1D. In control cells, the nucleus was stained blue, whereas no red fluorescence was observed. In the presence of 50 μM 4″-alkyl EGCG derivatives or EGCG, red fluorescence was observed, which indicated that the cells are undergoing apoptosis. 4″-C_{12} EGCG, 4″-C_{14} EGCG, and 4″-C_{16} EGCG treatment groups showed maximum cell death as compared to other 4″-alkyl EGCG derivatives. A Hoechst 33342/PI cytological study suggested that 4″-alkyl EGCG derivatives, along with EGCG and Gefitinib (5 μM), induce cytotoxicity in U87-MG cells.

3.2. 4″-Alkyl EGCG Derivatives Induce Apoptosis in GBM Cells. To evaluate the detailed mechanism behind the 4″-alkyl EGCG derivatives-induced cell death, we performed Western blot and flow cytometry analysis. Western blot analysis revealed that the expression level of the antiapoptotic marker BCL_{XL} was significantly downregulated by 50 μM of 4″-C_{12} EGCG and 4″-C_{14} EGCG (Figure 2A). From the obtained graph, it is evident that 4″-alkyl EGCG derivatives, particularly 4″-C_{12} EGCG and 4″-C_{14} EGCG, were able to inhibit cell growth and apoptosis induction in GBM cells (Figure S1A in Supporting Information). To further assess whether the activation of caspase-3 was involved in inducing apoptosis, we checked the expression of cleaved caspase-3 upon 24 h treatment of 4″-alkyl EGCG derivatives in U87-MG cells. As shown in the graph (Figure S1B in Supporting Information), cleaved caspase-3 expression can be seen in the Gefitinib-, EGCG-, 4″-C_{10} EGCG-, 4″-C_{12} EGCG-, and 4″-C_{14} EGCG-treated groups. Interestingly, maximum cleavage of caspase-3 was observed in 4″-C_{14} EGCG, which also resembled the BCL_{XL} results.

Next, to support the Western blot results and to unravel the mechanism of 4″-alkyl EGCG-mediated cell growth inhibition, the apoptotic rate was measured by annexin V/PI staining. Fluorescence-activated cell sorting (FACS) analysis showed that early and late apoptotic cell death occurred after 4″-alkyl EGCG treatment (Figure 2B). Consistent with Western blot results, the 4″-C_{12} EGCG (42.82%) and 4″-C_{14} EGCG (36.89%) treated groups showed the maximum apoptosis rate among the 4″-alkyl EGCG derivatives. However, the EGCG- and Gefitinib-treated group showed the 14.04 and 44.16% apoptosis rate, respectively. Furthermore, it is well established that during the early phase of apoptosis, both caspase-3 and BCL_{XL} are actively involved, which strongly suggests that 4″-alkyl EGCG treatment-induced apoptosis mainly through the early stage of apoptosis.

3.3. 4″-Alkyl EGCG Derivatives Inhibited the Phosphorylation of EGFR. The signaling pathways activated by EGFR autophosphorylation include activation in the EGFR-Ras-Raf-c-Jun N-terminal (JNK), EGFR-PI3K/protein kinase B (AKT)/mechanistic target of rapamycin (mTOR), and EGFR-Janus kinase (JAK)-signal transducer and activator of transcription-3 (STAT3) signaling pathways, and all of them have regulatory effects on autophagy.[65] EGFR also can trigger the tyrosine kinase phosphorylation of Beclin1 at Y229, Y233, and Y352 amino acid residues, leading to the formation of Beclin1 homodimers and thus inhibiting the autophagy.[66] In addition, EGFR also activates the AKT/mTOR pathway, which is also a negative regulator of autophagy.[67]

These prompted us to hypothesize that there is a strong link between EGFR and autophagy, and hence, we went ahead to explore the inhibitory effect of 4″-alkyl EGCG derivatives against phospho-EGFR. Wherein, U87-MG cells were exposed to 50 μM 4″-alkyl EGCG derivatives for 1, 4, and 24 h, followed by EGF stimulation (50 ng/mL) for 15 min. The phosphor-

https://doi.org/10.1021/acsomega.3c06110
ACS Omega 2024, 9, 2286−2301

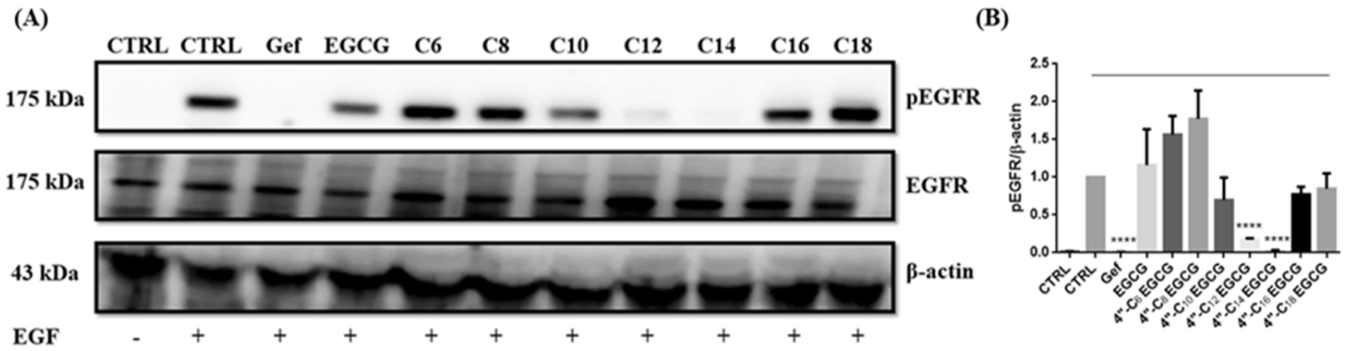

Figure 3. 4″-Alkyl EGCG derivatives inhibited the EGF-stimulated phosphorylation of EGFR. (A) U87-MG cells were treated with 5 μM Gefitinib and 50 μM of EGCG and 4″-alkyl EGCG derivatives for 24 h; then, the inhibition of phosphorylation level of EGFR was analyzed by Western blot analysis. (B) Intensity of pEGFR bands was quantified and shown as a relative expression level after being normalized by β-actin. All these data were represented as mean ± SEM, where $n = 3$. (*$P < 0.1$, **$P < 0.05$, ***$P < 0.01$, and ****$P < 0.001$ versus control).

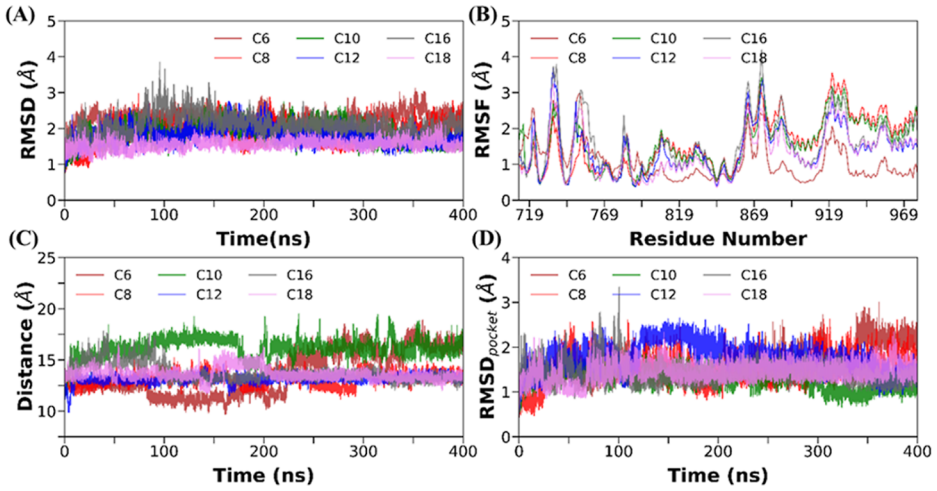

Figure 4. Structural stability and flexibility of WT EGFR bound with 4″-alkyl EGCG derivatives (A) time evolution of root means squared deviation (RMSD) of backbone atoms EGFR complexes relative to their respective equilibrated position, (B) root mean squared fluctuations (RMSFs) of C_α atoms for all six complexes, (C) center of mass distance between the binding pocket of EGFR kinase and the ligand molecules, and (D) RMSD of backbone atoms the binding pocket residues for all six complexes.

ylation level of EGFR was assessed by Western blot analysis. We conducted the Western blot analysis to assess the inhibitory profiling of 4″-alkyl EGCG derivatives at early time points (1 and 4 h). Western blot results indicated that 4″-alkyl EGCG derivatives (particularly 4″-C_{12} EGCG and 4″-C_{14} EGCG) were able to inhibit the EGF-stimulated phosphorylation of EGFR after 1 and 4 h of treatment (Figure S2 in Supporting Information). After 24 h of treatment, we observed that pEGFR expression was significantly downregulated by 5 μM of Gefitinib and 50 μM of 4″-C_{14} EGCG ($P < 0.1$) treatment (Figure 3B). In addition, 4″-C_{10} EGCG and 4″-C_{12} EGCG also inhibited the expression of pEGFR in U87-MG cells. However, these treatments caused no change in the basal EGFR level.

3.4. Analysis of the Binding Mode and the Interaction Profile of 4″-Alkyl EGCG Derivatives Against EGFR. To investigate the binding mode and interaction profiles, docking studies followed by MD were conducted between 4″-alkyl EGCG derivatives and EGFR. This study follows the same protocol as our previous study, where we conducted an MD simulation study on a similar system against 4″-C_{14} EGCG and EGCG to determine the binding mode and interaction profile.[40] Therefore, we decided to exclude 4″-C_{14} EGCG and EGCG in the current investigation. The XP module of the GLIDE module of the Schrodinger suite was used for the docking to estimate the primary binding pose of all 4″-alkyl EGCG derivatives with EGFR. The docking score and the binding pose of the main part of EGCG were estimated to be the same as found in our previous study.[40] We conducted 2 × 400 ns long MD simulations to estimate the stability of each docked complex. The root-mean-square deviation (RMSD) of all six complexes, calculated with respect to the equilibrium conformation, is shown in Figure 4A. A similar trend was observed for the replica simulation (data not shown). The average RMSDs for all complexes were found to vary between 1.0 and 2.0 Å for both runs. We also estimated the flexibility of each amino acid for all complexes by calculating the root-mean-square fluctuations (RMSF) with respect to the Cα atom, as shown in Figure 4B. The RMSF profiles for all complexes displayed a similar trend. However, in the presence of 4″-C_6 EGCG, EGFR becomes more rigid. However, the binding region remains stable compared to the flexible C terminal region and other functional regions, i.e., the P loop, A loop, and αC helix, indicating stable binding throughout the simulation length.

The strength of the binding mode was also estimated by determining the distance between the ligands and the center of mass of the binding pocket of equilibrated conformation, as shown in Figure 4C. In the case of 4″-C_{10} EGCG, the ligand showed a higher dynamic nature and reoriented from its

https://doi.org/10.1021/acsomega.3c06110
ACS Omega 2024, 9, 2286−2301

Table 1. Energetic Components of the Binding Free Energy for EGFR Complexed with Derivatives of EGCG, Estimated Using the MM-PBSA (kcal/mol) Method[a]

system	ΔE_{vdW}	ΔE_{elec}	ΔG_{pol}	ΔG_{np}	ΔE_{MM}[b]	ΔG_{solv}[c]	ΔG_{bind}[d]
4″-C_6 EGCG	−25.39 (0.71)	−19.89 (7.56)	28.97 (7.91)	−3.16 (0.14)	−45.29 (6.85)	25.80 (8.05)	−19.49 (1.20)
4″-C_8 EGCG	−55.82 (5.31)	−35.22 (15.13)	62.24 (14.18)	−5.84 (0.19)	−91.04 (9.82)	56.40 (13.99)	−34.64 (4.16)
4″-C_{10} EGCG	−48.29 (2.33)	−29.86 (3.30)	56.04 (1.32)	−5.58 (0.07)	−78.15 (0.96)	50.46 (1.39)	−27.69 (0.42)
4″-C_{12} EGCG	−62.40 (1.10)	−62.96 (2.18)	74.91 (0.45)	−6.36 (0.06)	−125.36 (1.08)	68.55 (0.50)	−56.81 (0.58)
4″-C_{16} EGCG	−56.38 (4.62)	−44.36 (2.47)	67.57 (2.05)	−6.38 (0.32)	−100.74 (2.15)	61.19 (1.74)	−39.55 (0.42)
4″-C_{18} EGCG	−61.53 (0.60)	−71.29 (9.82)	86.60 (8.97)	−7.09 (0.21)	−132.81 (9.22)	79.51 (9.17)	−53.31 (0.05)

[a]Standard deviations are provided in parentheses. [b]=$\Delta E_{vdW} + \Delta E_{elec}$. [c]=$\Delta G_{pol} + \Delta G_{np}$. [d]=$\Delta E_{vdW} + \Delta E_{elec} + \Delta G_{pol} + \Delta G_{np}$.

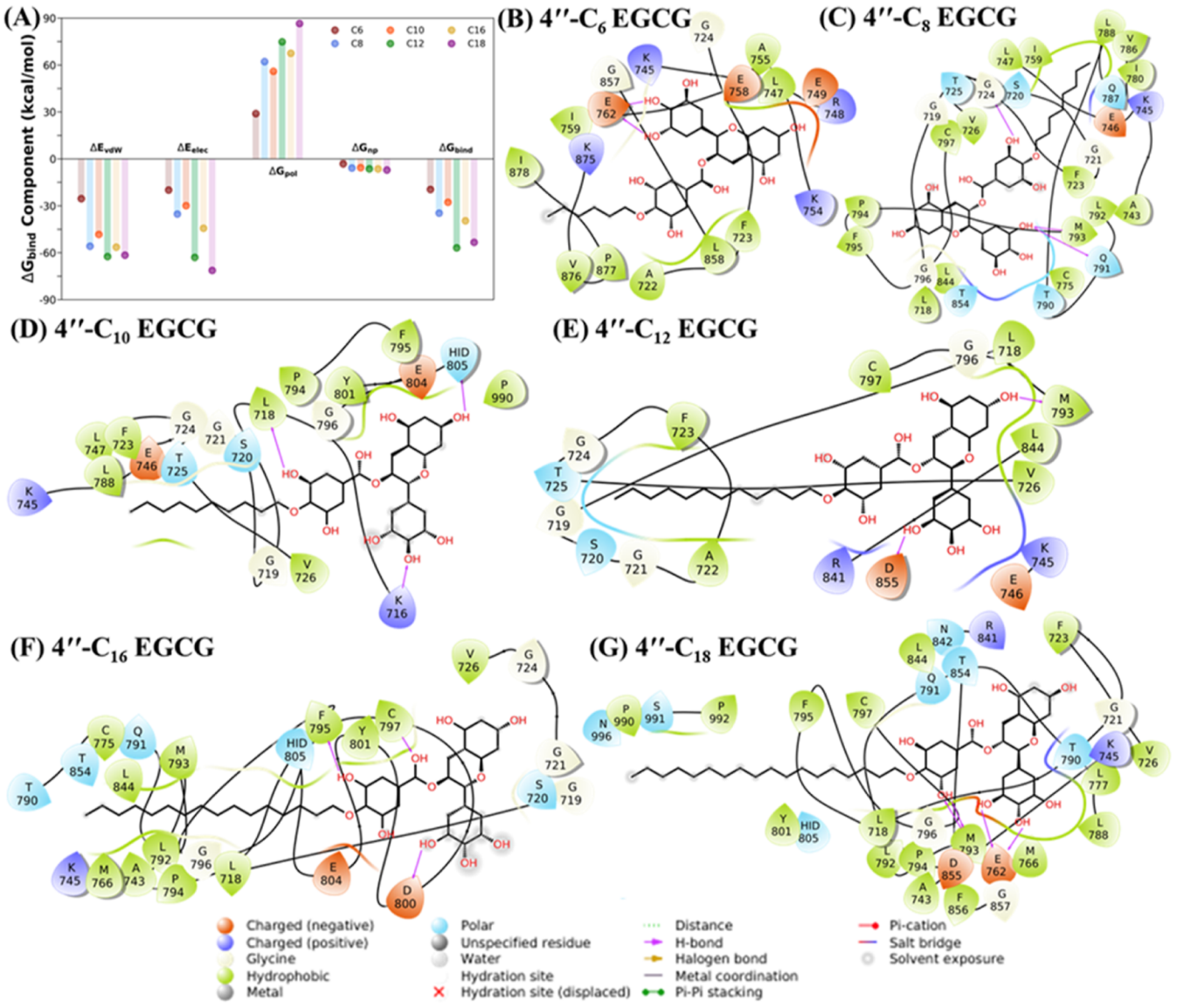

Figure 5. Energetic component analysis and 2D representation of ligand−protein interactions of different modifications of EGCG against WT EGFR. (A) Different components of binding free energies for all six different complexes (B) 4″-C_6 EGCG/EGFR, (C) 4″-C_8 EGCG/EGFR, (D) 4″-C_{10} EGCG/EGFR, (E) 4″-C_{12} EGCG/EGFR, (F) 4″-C_{16} EGCG/EGFR, and (G) 4″-C_{18} EGCG/EGFR.

equilibrium position, and after 200 ns, it shifted from the initial position and remained unstable throughout the simulation run, indicating the possibility of less binding affinity among other molecules. A similar observation was also seen in the time evolution of the RMSD of the binding pocket (5 Å surrounding the molecule) (as shown in Figure 4D), where 4″-C_6 shows a higher deviation after 300 ns.

To further elucidate the recognition process, we estimated the overall binding energy (ΔG_{bind}) and its different components by using the MMPBSA scheme for the last 200 ns of the trajectory. A summary of the binding free energy and its components, obtained by averaging both runs, is summarized in Table 1 and Figure 5. As it can be seen in Figure 5A, the polar solvation (ΔG_{pol}) disfavors the binding of 4″-alkyl EGCG derivatives,

https://doi.org/10.1021/acsomega.3c06110
ACS Omega 2024, 9, 2286−2301

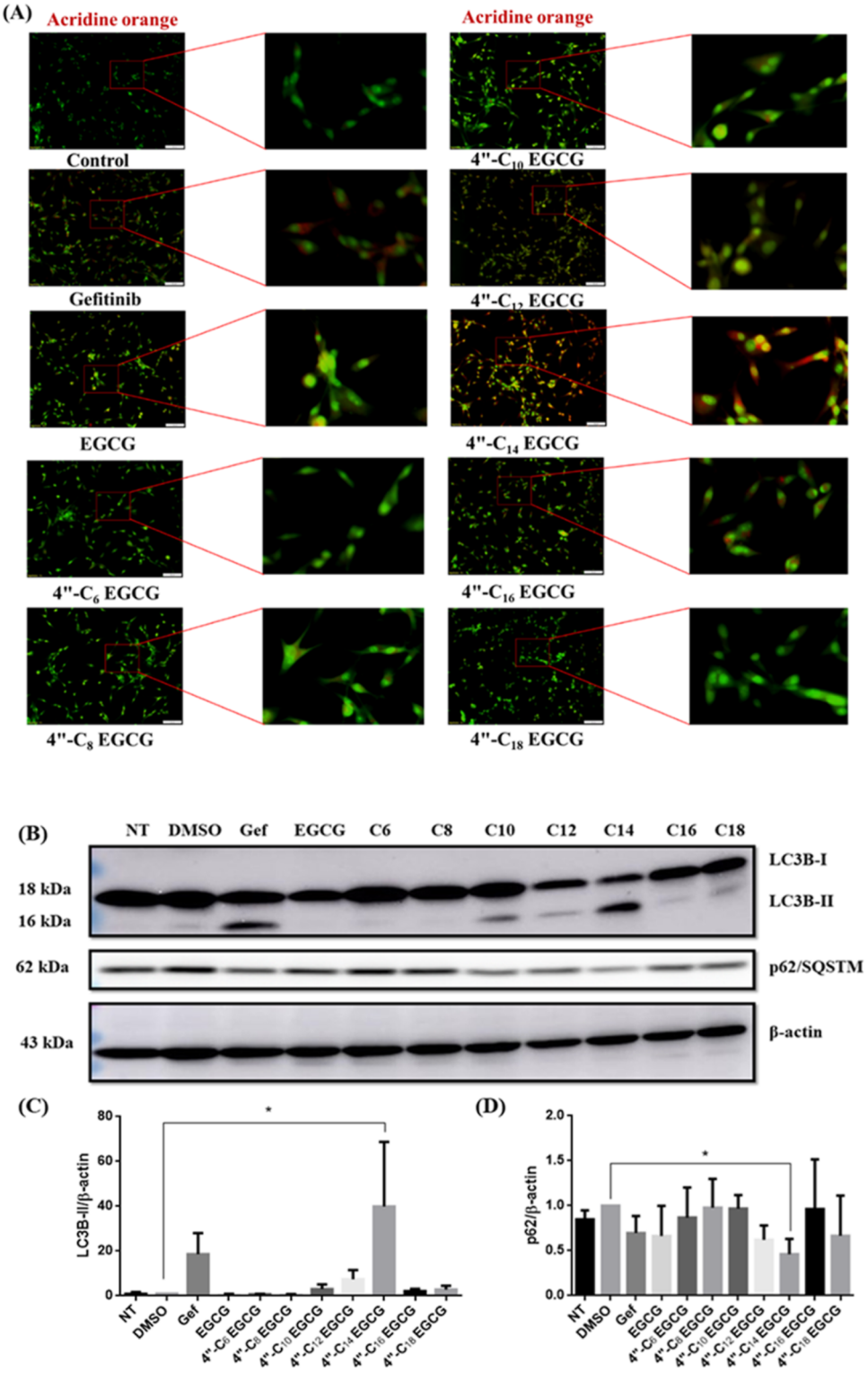

Figure 6. 4″-Alkyl EGCG derivatives induce autophagy in U87-MG cells. (A) U87-MG cells were treated with 5 μM Gefitinib and 50 μM of EGCG and 4″-alkyl EGCG derivatives for 24 h, followed by cells being stained with 10 μg/mL Acridine Orange at 37 °C for 15 min to check the presence of acridine orange-stained intracellular vesicles by fluorescent microscopy (B) U87-MG cells were treated with 5 μM Gefitinib, 50 μM EGCG, and 4″-alkyl EGCG derivatives for 24 h. Next, the autophagic markers, LC3 and p62/SQSTM1, were analyzed by Western blot analysis. (C and D) Intensity of the LC3 and p62/SQSTM1 bands was quantified and shown as a relative expression level after being normalized by β-actin. All these data were represented as mean ± SEM, where $n = 3$. (*$P < 0.1$ versus control).

while the rest of the components (ΔE_{vdW}, ΔE_{elec} and ΔG_{np}) showed a favorable nature toward bindings. Moreover, Table 1 revealed that 4″-C_{12} EGCG has the highest binding energy (−56.81 kcal/mol), and 4″-C_6 EGCG showed the lowest binding free energy (−19.49 kcal/mol). The increase in the electrostatic and lowering of the nonpolar contribution also makes 4″-C_{12} EGCG a better binding partner compared to 4″-C_{14} EGCG (−45.06 kcal/mol), as estimated in our previous

https://doi.org/10.1021/acsomega.3c06110
ACS Omega 2024, 9, 2286−2301

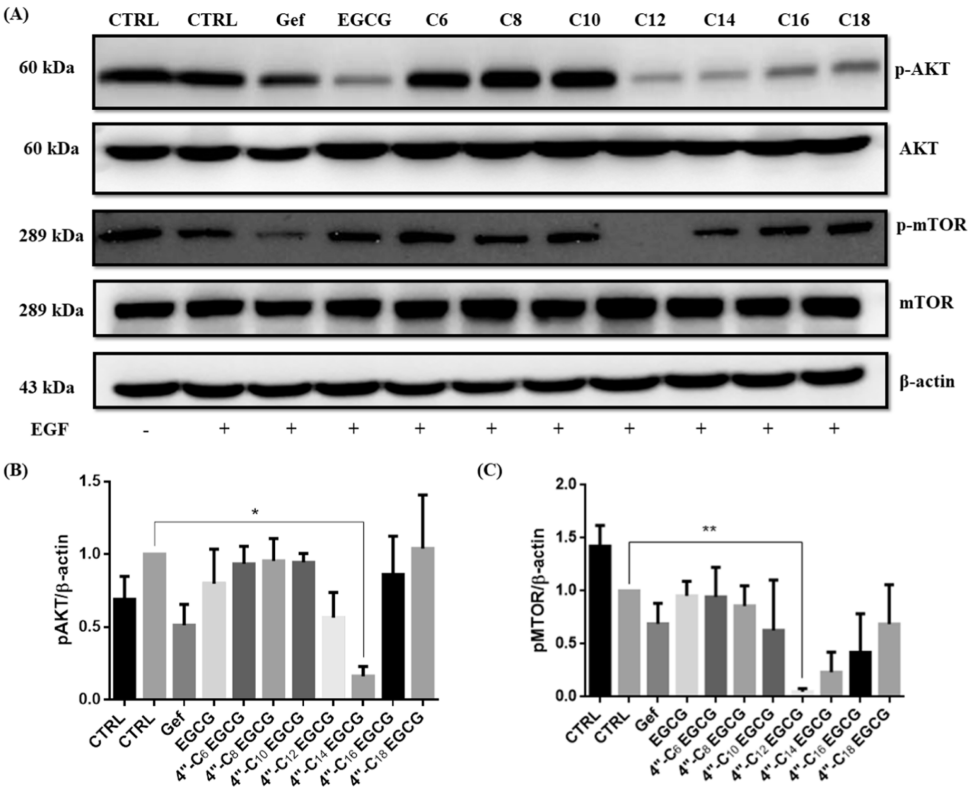

Figure 7. 4″-Alkyl EGCG derivatives activated autophagy by blocking the phosphorylation of the AKT/mTOR signaling pathway in U87-MG cells. (A)U87-MG cells were exposed to 5 μM Gefitinib and 50 μM of EGCG and 4″-alkyl EGCG derivatives for 24 h. Next, the expression of pAKT and *p*-mTOR was determined by Western blot analysis. (B and C) Intensity of pAKT and *p*-mTOR bands was quantified and shown as a relative expression level after being normalized by β-actin. All these data are represented as the mean ± SEM, where $n = 3$. (*$P < 0.1$, **$P < 0.05$, versus control).

work.[40] However, the 4″-C_{18} EGCG compound also showed a promising binding (−53.31 kcal/mol) in our study, which contradicts our experimental work. This may be possible because of its long chain, which may create additional contact with the protein. In the experimental conditions, the long chain hinders entry of the molecule into its target location, which results in decreased affinity in the interaction pattern.

Further, the interaction profiles for all of the complexes were estimated. Figure 5B−G shows several key interactions along with different key hydrogen bonds for all complexes. We also estimated the average occupancy of hydrogen bonds between protein and ligand and listed it in Table S1 in Supporting Information. In the case of 4″-C_{12} EGCG, four major hydrogen bonds (more than 50%) were observed involving residues E762, R841, L788, and D855 in the presence of the R842 complex, which makes it a prominent binding partner. This result also supports the higher increase of electrostatic contributions from the MMPBSA. E762 and D855 are the key residues found in cases of 4″-C_{12} EGCG, 4″-C_{16} EGCG, and 4″-C_{18} EGCG, which are also critical residues, as shown from the interaction analysis.

On the contrary, smaller alkyl chain derivatives showed differences in the hydrogen bonding profile regarding residue location and the strength of the hydrogen occupancy. This may signify the importance of the tail part, which may help the molecule reorient in a better way to achieve promising binding. Altogether, these studies suggest that an increase in the alkyl chain length provides structural stability for EGCG to interact with wild-type EGFR.

3.5. 4″-Alkyl EGCG Derivatives Induce Autophagy in GBM Cells. It has been reported that EGFR TKIs such as gefitinib, erlotinib, afatinib, and osimertinib treatment trigger autophagy in several cancer cells, including tongue cancer, lung cancer, and chronic myeloid leukemia, and more importantly, this autophagy induction is currently believed to be an important cause of drug resistance.[68,69] From the previous research, it was confirmed that 4″-C_{14} EGCG inhibited the autophosphorylation of EGFR,[40] therefore, we hypothesized that autophagy might be activated in tumor cells that were exposed to 4″-alkyl EGCG derivatives, as after blockade of EGFR, several TKIs have induced protective autophagy. Thus, we evaluated whether autophagy can be induced by the 4″-alkyl EGCG derivatives, EGCG and Gefitinib, in U87-MG cells. In preliminary studies, we employed acridine orange (AO), a dye which emits red fluorescence in acidic vesicles and green fluorescence in nonacidic vesicles. We have found that treatment of U87-MG cells with 4″-alkyl EGCG derivatives causes the accumulation of AO-stained orange-red acidic vesicles resembling autolysosomes (Figure 6A). Next, to confirm the induction of autophagy by 4″-alkyl EGCG derivatives, the switch of LC3-I into LC3-II before and after 4″-alkyl EGCG derivative treatment was determined by Western blot analysis. LC3 (microtubule-associated protein 1A/1B-light chain 3) and p62/SQSTM1 are the two important hallmarks of autophagy. LC3 exists in two cellular forms: LC3-I (cytoplasmic) and LC3-II (membrane-bound). During autophagy, LC3-I converts into LC3-II, and the amount of LC3-II becomes an important marker to study the formation of autophagosomes.[70] We also determined the expression of the autophagic flux marker p62/SQSTM1, which gets down-regulated during autophagy.[71] Results from Western blot analysis (Figure 6B) showed that 4″-C_{14} EGCG significantly increased the conversion of LC3-I to the characteristic autophagy induction marker LC3-II in U87-MG cells after 24

https://doi.org/10.1021/acsomega.3c06110
ACS Omega 2024, 9, 2286−2301

h of treatment. Moreover, 4″-C_{10} EGCG, 4″-C_{12} EGCG, and Gefitinib (positive control) were also able to induce autophagy through the transformation of LC3-I to LC3-II. As can be seen from Figure 6C, no conversion of LC3-I to LC3-II was observed in U87-MG cells treated by EGCG, 4″-C_6 EGCG, and 4″-C_8 EGCG but comparatively increased conversion of LC3-II can be seen from 50 μM of 4″-C_{10} EGCG to 4″-C_{14} EGCG treatment group, where 4″-C_{14} EGCG showed the maximum conversion. Interestingly, increasing chain length at the 4″ position of EGCG could be the plausible reason for this result.

To deeply uncover the underlying mechanism behind autophagy induction by 4″-alkyl EGCG derivatives in U87-MG cells, we determined the autophagic flux by checking the expression of p62/SQSTM1, a specific protein for autophagy degradation, in the course of 4″-alkyl EGCG derivative treatment. Western blot analysis showed that 50 μM of 4″-C_{14} EGCG markedly suppressed the expression of p62 in the U87-MG cell line (Figure 6D). In addition, Gefitinib, 4″-C_{10} EGCG, and 4″-C_{12} EGCG were also able to partially downregulate p62 expression. All the above results strongly suggest that autophagy can be triggered by Gefitinib, 4″-C_{10} EGCG, 4″-C_{12} EGCG, and 4″-C_{14} EGCG in U87-MG cells, while these compounds also inhibited the autophosphorylation of EGFR. These findings indicated that autophagy induction in the U87-MG cell line is associated with EGFR inhibition by 4″-alkyl EGCG derivatives.

3.6. 4″-Alkyl EGCG-Induced Autophagy Associated with the Inhibition of AKT/mTOR Signaling Cascade. Apart from the effect on cancer cell proliferation, the AKT/mTOR pathway is also involved in the regulation of autophagy.[30] Earlier studies have also confirmed that the AKT/mTOR signaling pathway acts as a negative regulator of autophagy.[29] To unravel the molecular mechanism behind 4″-alkyl EGCG derivatives-mediated autophagy induction, we investigated the activation status of this autophagy suppressive signaling pathway. As evident from Figure 7, phosphorylation of AKT and mTOR significantly decreased in U87-MG upon 24 h treatment with mainly 4″-C_{12} EGCG and 4″-C_{14} EGCG ($P < 0.1$). However, Gefitinib and 4″-C_{16} EGCG were also potent in inhibiting p-mTOR and p-AKT. On the other hand, 50 μM concentrations of 4″-C_{12} EGCG ($P < 0.1$) and 4″-C_{14} EGCG inhibited the EGF-stimulated phosphorylation of mTOR. Gefitinib and 4″-C_{16} EGCG were also able to downregulate p-mTOR expression in U87-MG cells (Figure 7). The decreased phosphorylation of AKT and mTOR provides compelling evidence that 4″-alkyl EGCG derivatives induce autophagy through the AKT/mTOR pathway.

3.7. 4″-Alkyl EGCG Derivatives Selectively Inhibited the Kinase Activity of Mutant EGFR over WT EGFR. The therapeutic efficacy of EGFR-TKIs has been restricted due to their acquired drug resistance. The common mechanism behind the acquired drug resistance is a gatekeeper mutation T790M, which further leads to a cancer initiation mutation, L858R.[72] Clinical investigations have revealed that the T790M/L858R resulted in reduced therapeutic benefits of EGFR-TKIs.[24] We were interested in validating the effectiveness of 4″-alkyl EGCG toward T790M/L858R EGFR. To elucidate the inhibition ability of 4″-alkyl EGCG against EGFR T790M/L858R and WT EGFR was carried out with three best 4″-alkyl EGCG derivatives (4″-C_{10} EGCG, 4″-C_{12} EGCG, and 4″-C_{14} EGCG) which were able to inhibit the EGF-stimulated autophosphorylation of EGFR in the U87-MG. In this experiment, EGCG was used as a reference compound, and gefitinib and WZ4002 were taken as positive controls. The obtained results are shown in Table 2 and

Table 2. Kinase Inhibitory Activity of 4″-Alkyl EGCG Derivatives on WT EGFR and T790M/L858R EGFR In Vitro[a]

compound name	IC_{50} (nM) EGFR-WT	IC_{50} (nM) EGFR (T790M/L858R)	selectivity index
Gefitinib (1st generation EGFR-TKI)	44.69 ± 0.07	59.21 ± 0.05	0.75
WZ4002 (3rd generation EGFR-TKI)	51.32 ± 0.12	7.98 ± 0.06	6.43
EGCG	115.2 ± 0.07	118.0 ± 0.07	0.97
4″-C_{10} EGCG	169.1 ± 0.15	103.8 ± 0.08	1.62
4″-C_{12} EGCG	21.46 ± 0.05	18.39 ± 0.09	1.16
4″-C_{14} EGCG	49.90 ± 0.05	33.33 ± 0.08	1.49

[a]The IC_{50} values are expressed as (mean ± SEM).

Figure S3A−L in Supporting Information. Among the screened compounds, 4″-C_{12} EGCG and 4″-C_{14} EGCG potently inhibited the kinase activity of L858R/T790M and WT EGFR with IC_{50} values of 18.39, 33.33, and 21.46 nM, 49.90, respectively. Additionally, 4″-C_{10} EGCG also showed promising kinase inhibitory activity for T790M/L858R EGFR (IC_{50} = 103.8 nM), compared to that of WT EGFR (IC_{50} = 169.1 nM). However, EGCG showed an almost similar inhibitory profile against T790M/L858R and WT EGFR, with IC_{50} values of 118 and 115.2 nM. Obtained results from the kinase assay indicated that the introduction of an alkyl chain at the 4″ position of EGCG enhanced the structural framework of EGCG, resulting in selectivity indexes of 1.69, 1.16, and 1.49 for 4″-C_{10} EGCG, 4″-C_{12} EGCG, and 4″-C_{14} EGCG, respectively, toward mutant EGFR (T790M/L858R) over WT EGFR.

3.8. 4″-Alkyl EGCG Showed Increased Binding Affinity with Mutant EGFR. In addition to the kinase assay, we also used the same computational protocol to determine the binding strength of the T790M/L858R EGFR with 4″-alkyl EGCG (4″-C_{10} EGCG, 4″-C_{12} EGCG, and 4″-C_{14} EGCG) and EGCG. The location of the mutant residues (T790 M and L858R) is shown in the crystal structure in ribbon style (Figure 8A). The structural stability and flexibility of all complexes were assessed over a 400 ns simulation period by calculating the root-mean-square deviation (RMSD) and root-mean-square flexibility (RMSF) (Figure 8B,C). All four complexes remained stable throughout the simulation period, enabling us to calculate the binding free energy. The stability of the ligands within the binding cavity was evaluated by measuring the center of mass distance between T790M/L858R EGFR and 4″-alkyl EGCG derivatives, and it was found to be maintained in all the cases. However, among complexes, 4″-C_{12} EGCG and 4″-C_{14} EGCG displayed greater stability. In the case of T790M/L858R EGFR, the ATP binding pocket showed greater flexibility compared to the WT EGFR conformation (Figure 8). The binding pockets showed stability in their flexibility after 100 ns, and 4″-C_{12} EGCG and 4″-C_{14} EGCG demonstrated comparatively lower conformational deviation compared to EGCG and 4″-C_{10} EGCG.

The MMPBSA estimation scheme supports the observation that the 4″-C_{10} EGCG, 4″-C_{12} EGCG, and 4″-C_{14} EGCG strongly bind to the T790M/L858R EGFR, with binding free energies of −43.18, −48.17, and −49.37 kcal/mol, respectively (Table 3). Contrarily, EGCG showed weak interaction toward the T790M/L858R EGFR complex with a binding free energy of −26.13 kcal/mol. Overall in silico results is also in agreement

https://doi.org/10.1021/acsomega.3c06110
ACS Omega 2024, 9, 2286−2301

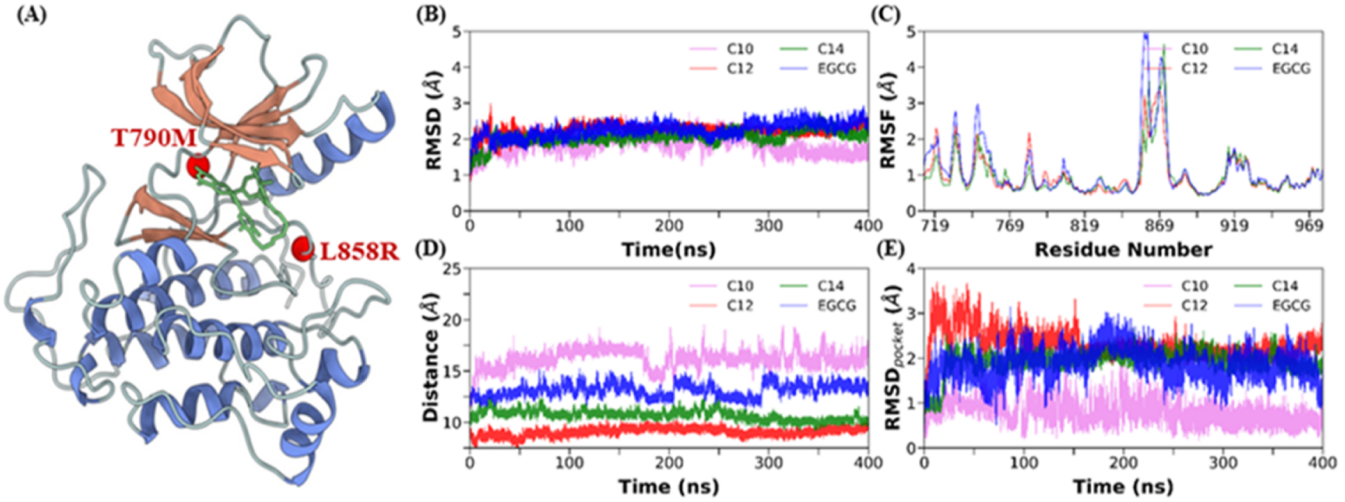

Figure 8. Structural stability and flexibility of T790M/L858R EGFR complexed with 4″-alkyl EGCG derivatives. (A) Location of the mutant residues (T790M and L858R) in EGFR, (B) time evolution of root means squared deviation (RMSD) of backbone atoms mutant EGFR complexes relative to their respective equilibrated position, (C) root mean squared fluctuations (RMSFs) of C_α atoms for all four complexes, (D) center of mass distance between the binding pocket of EGFR kinase and the ligand molecules, and (E) $RMSD_{pocket}$ of backbone atoms, the binding pocket residues for all four complexes.

Table 3. Energetic Components of the Binding Free Energy for T790M/L858R EGFR Bound with 4″-Alkyl EGCG Derivatives, Estimated Using the MM-PBSA (kcal/mol) Method[a]

system	ΔE_{vdW}	ΔE_{elec}	ΔG_{pol}	ΔG_{np}	ΔE_{MM}[b]	ΔG_{solv}[c]	ΔG_{bind}[d]
EGCG	−41.66 (5.01)	−34.05 (9.69)	53.87 (3.37)	−4.48 (0.13)	−75.72 (4.68)	49.39 (3.25)	−26.33 (1.43)
4″-C_{10} EGCG	−53.32 (11.12)	−62.52 (12.82)	78.81 (4.48)	−6.15 (0.18)	−115.84 (1.70)	72.66 (4.67)	−43.18 (2.97)
4″-C_{12} EGCG	−60.72 (10.93)	−59.08 (18.22)	78.14 (4.99)	−6.5 (0.28)	−119.81 (7.28)	71.64 (5.27)	−48.17 (2.01)
4″-C_{14} EGCG	−62.78 (5.73)	−56.45 (27.87)	77.01 (22.28)	−7.16 (0.13)	−119.23 (22.14)	69.85 (22.41)	−49.37 (0.27)

[a]Standard deviations are provided in parentheses. [b]=$\Delta E_{vdW} + \Delta E_{elec}$. [c]=$\Delta G_{pol} + \Delta G_{np}$. [d]=$\Delta E_{vdW} + \Delta E_{elec} + \Delta G_{pol} + \Delta G_{np}$.

with the experimental findings and suggest that 4″-alkyl EGCG derivatives are mutant selective EGFR-TKIs. The interaction profiles for all of the complexes were estimated. Figure S4A−D in the Supporting Information shows several key interactions along with different key hydrogen bonds for all the complexes.

3.9. Inhibition of Cytoprotective Autophagy by CQ Sensitizes 4″-Alkyl EGCG Derivatives-Induced GBM Cell Death. Studies have proven that autophagy plays a protective role in cancer cells during antitumor drug administration, including TKIs, DNA-damaging agents, and radiation therapies.[73] However, suppression of protective autophagy can increase drug-induced cancer cell death through apoptosis.[73] To investigate the role of autophagy triggered by 4″-C_{10} EGCG, 4″-C_{12} EGCG, and 4″-C_{14} EGCG, a well-established autophagy inhibitor CQ was employed to cotreat U87-MG cells. We assessed the effect of cotreatment on U87-MG growth inhibition. It is well known that CQ inhibits downstream autophagy and enhances LC3-II expression levels by aggregation of the autophagosome.[68] It is evident from Figure 9A that CQ significantly increases Gefitinib and 4″-C_{14} EGCG-mediated conversion of LC3-II. Co-incubation of CQ with 4″-C_{12} EGCG also led to enhanced transformation of LC3-II, while no alteration was observed in the 4″-C_{10} EGCG and CQ treatment group.

We also examined the cytotoxicity effect of EGCG, 4″-C_{10} EGCG, 4″-C_{12} EGCG, and 4″-C_{14} EGCG with and without autophagy inhibition by CQ using the CCK-8 assay. It can be seen from Figure 9C, CQ, along with the aforementioned 4″-alkyl EGCG derivatives, significantly augmented U87-MG cell death. Consistent with Western blot results, a maximum growth inhibitory effect was observed at 50 μM of 4″-C_{14} EGCG cotreated with the CQ group with 77.08%, while alone it showed 45.18% cytotoxicity after 24 h of treatment ($P < 0.001$). CCK-8 assay results revealed that blocking autophagy by CQ further significantly enhanced the EGCG (66.82%)- and 4″-C_{10} EGCG (54.80%)-mediated cell death compared to being treated alone, where it showed 39.10 and 13.89% cell death, respectively. While Gefitinib and 4″-C_{12} EGCG, along with CQ, showed only 2.09 and 4.3% increase in cell death as compared with the treated alone group (Figure 9C), respectively. From these results, it was confirmed that blockage of autophagy significantly improves the anticancer activity of 4″-alkyl EGCG derivatives and EGCG.

3.10. 4″-Alkyl EGCG Exhibited Strong Binding with the Drug Transporter Protein HSA. Human serum albumin (HSA) is the most abundant monomeric multidomain protein found in plasma and plays a crucial role in drug transportation via the bloodstream to the target cells.[74,75] The interaction of the drugs with HSA leads to a change in their metabolism, distribution, and concentration.[76] Moreover, HSA also enhances the solubility of the medications in plasma, minimizes toxicity, and prevents from oxidation.[77] Fluorescence spectrophotometry techniques have commonly been used to study the molecular interaction of compounds with albumins.[78,79] Tyrosine, tryptophan, and phenylalanine are the three residues responsible for the autofluorescence activity of HSA. HSA consists of 585 amino acids, including a single tryptophan residue (Trp 214), which is responsible for generating fluorescence.[80]

Therefore, we decided to study the interaction profile of the three best 4″-alkyl EGCG derivatives (4″-C_{10} EGCG, 4″-C_{12} EGCG, and 4″-C_{14} EGCG) and EGCG with the drug

https://doi.org/10.1021/acsomega.3c06110
ACS Omega 2024, 9, 2286−2301

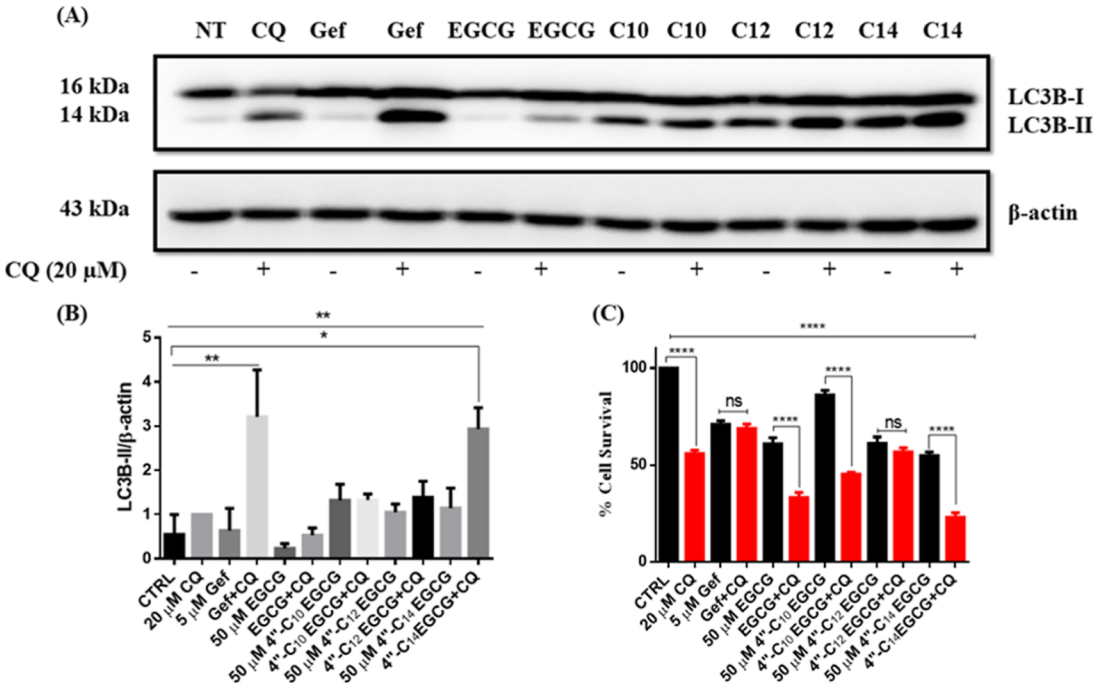

Figure 9. Blockade of autophagy increases the cytotoxicity of 4″-alkyl EGCG derivatives in GBM cells. (A) U87-MG cells were treated with 5 μM Gefitinib and 50 μM of EGCG and 4″-C_{10} EGCG, 4″-C_{12} EGCG, and 4″-C_{14} EGCG for 24 h with or without 20 μM CQ. Next, the autophagic markers, LC3, were analyzed by Western blot analysis. (B) Intensity of LC3 bands was quantified and shown as the relative expression level after being normalized by β-actin. (C) Viability of U87-MG cells incubated with 5 μM Gefitinib and 50 μM of EGCG and 4″-C_{10} EGCG, 4″-C_{12} EGCG, and 4″-C_{14} EGCG for 24 h with or without 20 μM CQ determined by the CCK-8 assay. All these data are represented as mean ± SEM, where $n = 3$. (*$P < 0.1$, **$P < 0.05$, ***$P < 0.01$, and ****$P < 0.001$ versus control).

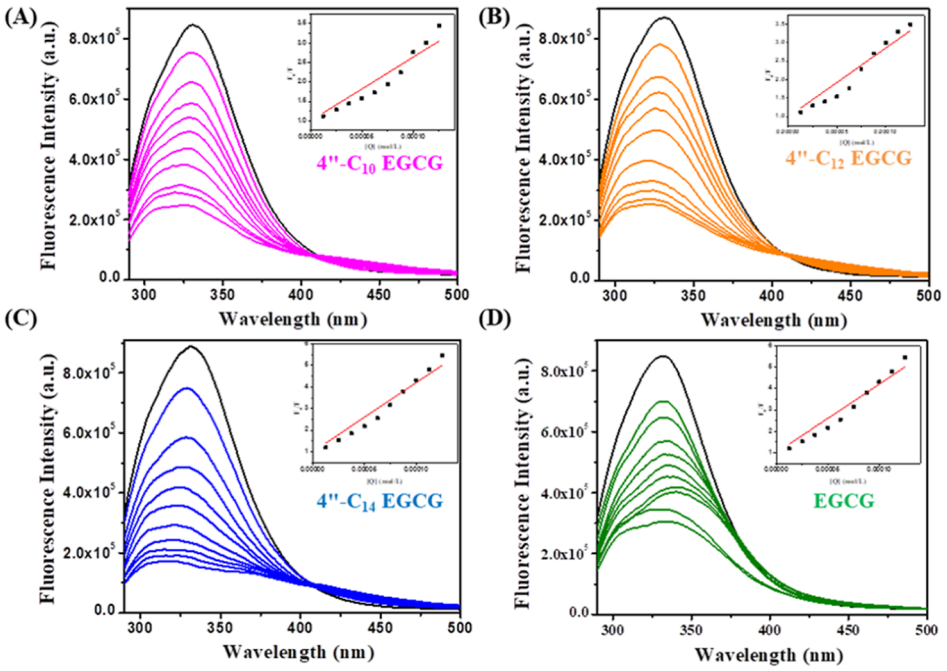

Figure 10. Fluorescence quenching spectra of HSA upon gradual addition of 4″-alkyl EGCG (A) 4″-C_{10} EGCG, (B) 4″-C_{12} EGCG, (C) 4″-C_{14} EGCG, and (D) EGCG. Inset: Stern-Volmer plot of HSA interacting with 4″-alkyl EGCG.

transporter protein HSA. Herein, we carried out the emission-quenching assay by gradually increasing the concentration (12.5 to 125 μM) of the 4″-alkyl EGCG derivatives to a fixed amount of HSA (10 μM) and observed a strong decrease in the emission-maxima at 345 nm with respect to increasing the concentration. The quenching constants for EGCG, 4″-C_{10} EGCG, 4″-C_{12} EGCG, and 4″-C_{14} EGCG were found to be 1.2×10^4, 1.6×10^4, 1.8×10^4, and 3.2×10^4, respectively, and these results indicate the interaction profile of HSA with EGCG and 4″-alkyl EGCG derivatives (Table S2 in Supporting Information). Additionally, we also determined the bimolecular quenching rate constant (K_q) of HSA with 4″-alkyl EGCG derivatives by using the

https://doi.org/10.1021/acsomega.3c06110
ACS Omega 2024, 9, 2286−2301

equation $K_{SV} = K_q \times \tau_0$, where τ_0 stands for the average decay lifetime of HSA in the absence of a quencher. The obtained Kq values for EGCG, 4″-C_{10} EGCG, 4″-C_{12} EGCG, and 4″-C_{14} EGCG were observed to be 1.9×10^{12}, 2.6×10^{12}, 2.9×10^{12}, and 5.17×10^{12}, respectively. Hypsochromic shift was observed in all four complexes, as can be seen from Figure 10; this could be due to the association of these compounds with the Trp residue of HSA. Among the tested derivatives, maximum binding affinity was observed for the 4″-C_{14} EGCG.

4. DISCUSSION

EGFR, upstream of the PI3K/AKT/mTOR pathway, plays a vital role in the cell proliferation, differentiation, and migration of cancer cells.[65] Thus, targeting EGFR by TKIs or monoclonal antibodies (mAbs) has become an important strategy for anticancer therapy. Several first, second, third, and now fourth-generation EGFR TKIs have been developed to block the EGFR. But the continuous mutation in EGFR (T790M, L858R, and C797S) causes acquired and natural resistance against the targeted therapy; however, other mechanisms of resistance are still being investigated.[65] Signaling pathways downstream of EGFR, such as PI3K/AKT/mTOR, are well-known to be associated in the regulation of autophagy, suggesting an important cross talk between EGFR inhibition and autophagy.[67] Thus, pharmacological or genetic inhibition of autophagy became an important approach to overcome drug resistance. In this study, we explored the efficacy of 4″-alkyl EGCG in inhibiting EGF-stimulated phosphorylation of the EGFR/AKT/mTOR signaling pathway by Western blot analysis. From the Western blot analysis, we observed that two derivatives of EGCG, namely, 4″-C_{12} EGCG and 4″-C_{14} EGCG, markedly inhibited the expression of pEGFR, pAKT, and p-mTOR in the U87-MG cell line. We found that 4″-C_{12} EGCG and 4″-C_{14} EGCG were more selective against inhibiting the kinase activity of double mutant EGFR (L858R/T790M) over WT EGFR through an in vitro kinase assay. By utilizing molecular docking and MD simulation studies, we also investigated the binding mode of these derivatives against WT EGFR and mutant EGFR (L858R/T790M) and found that an increase in the alkyl chain length provides structural stability for EGCG to interact with EGFR. Taken together, our study demonstrated that EGFR/Akt/mTOR pathway inhibition might contribute to 4″-alkyl EGCG-induced autophagy in U87-MG. These derivatives were also potent in augmenting cell death and apoptosis induction.

Autophagy plays a vital role in cancer cells for the transportation of degraded cellular organelles and aggregated proteins, while it is also involved in the maintenance of energy production, which causes cancer progression and resistance to therapy.[81] Antitumor therapies such as chemotherapy and radiotherapy have been found to activate autophagy in GBM.[82] From the currently available studies, it is evident that cancer cell autophagy causes adaptive response mediating resistance to several first, second, and third generations of EGFR TKIs, such as gefitinib,[41,83] erlotinib,[84] afatinib,[68] osimertinib,[85] and inhibition of cytoprotective autophagy results in enhanced sensitivity and effectiveness of these EGFR-TKIs. On the other hand, several plant-derived natural compounds have been proposed for drug discovery for many years as potent anticancer agents. Among them, multiple natural compounds have already shown great therapeutic response in reversing drug resistance caused by induction of cytoprotective autophagy.[86,87] Regulation of autophagy by natural compounds can be a potential therapeutic approach for overcoming the drug resistance.[86] In the present study, we showed that LC3-I to LC3-II conversion and p62/SQSTM1 inhibition in 4″-alkyl EGCG-treated U87-MG cells were observed with respect to untreated cells. These findings provide an important insight that 4″-alkyl EGCG treatment induces autophagy in GBM cells upon EGFR blockade.

Numerous preclinical research works demonstrate that the blockade of autophagy by CQ or 3-MA is recently being considered as a new therapeutic strategy for anticancer agents.[88] The blockage of autophagy improves the effectiveness of EGFR-TKIs.[88] We have found that cotreatment of GBM cells with Gefitinib, EGCG, 4″-C_{10} EGCG, 4″-C_{12} EGCG, or 4″-C_{14} EGCG, along with CQ, resulted in increased cytotoxicity of these compounds.

5. CONCLUSIONS

In conclusion, these findings provide an insightful result that tumor cells may survive in stress conditions following blockage of the EGFR-mediated signaling pathways by inducing autophagy. But, in combination with a pharmacological inhibitor of autophagy, it can again inhibit cancer cell growth with enhanced efficacy. Our study also provides a separate strategy of EGFR inhibition by natural compound-based derivatives with improved anticancer efficacy, wherein 4″-alkyl EGCG derivatives also resulted in the mutant EGFR (T790M/L858R) inhibition. Taken together, our findings highlight that the combination of 4″-alkyl EGCG and the autophagy inhibitor can be a promising approach to overcome the autophagy-mediated drug resistance and improve sensitivity against cancer cells.

■ ASSOCIATED CONTENT

Supporting Information

The Supporting Information is available free of charge at https://pubs.acs.org/doi/10.1021/acsomega.3c06110.

Binding mode and interaction profile of 4″-alkyl EGCG derivatives against WT EGFR, interaction profile of the 4″-alkyl EGCG with HSA, decomposition of the binding free energy into contributions from individual residues, 4″-Alkyl EGCG derivatives-triggered apoptosis in U87-MG cells, 4″-Alkyl EGCG derivatives-mediated EGFR inhibition at early time points, kinase inhibitory activities of 4″-alkyl EGCG derivatives against WT-EGFR and T790M/L858R EGFR, 2D representation of ligand−protein interactions against T790M/L858R EGFR, and uncropped Western blot images and methodology of protein binding study (PDF)

■ AUTHOR INFORMATION

Corresponding Authors

Avinash Sonawane − *Department of Biosciences and Biomedical Engineering, Indian Institute of Technology Indore, Indore, Madhya Pradesh 453 552, India;* orcid.org/0000-0002-9596-2629; Email: asonawane@iiti.ac.in

Sushabhan Sadhukhan − *Department of Chemistry, Indian Institute of Technology Palakkad, Palakkad, Kerala 678 623, India;* orcid.org/0000-0002-3302-5875; Email: sushabhan@iitpkd.ac.in

https://doi.org/10.1021/acsomega.3c06110
ACS Omega 2024, 9, 2286−2301

Authors

Satyam Singh − *Department of Biosciences and Biomedical Engineering, Indian Institute of Technology Indore, Indore, Madhya Pradesh 453 552, India*

Priya Ghosh − *Department of Biosciences and Biomedical Engineering, Indian Institute of Technology Indore, Indore, Madhya Pradesh 453 552, India*

Rajarshi Roy − *Department of Biosciences and Biomedical Engineering, Indian Institute of Technology Indore, Indore, Madhya Pradesh 453 552, India*

Ananyaashree Behera − *School of Biotechnology, KIIT Deemed to be University, Bhubaneswar, Orissa 751 024, India*

Revathy Sahadevan − *Department of Chemistry, Indian Institute of Technology Palakkad, Palakkad, Kerala 678 623, India;* orcid.org/0000-0001-5789-5499

Parimal Kar − *Department of Biosciences and Biomedical Engineering, Indian Institute of Technology Indore, Indore, Madhya Pradesh 453 552, India;* orcid.org/0000-0001-8451-9739

Complete contact information is available at: https://pubs.acs.org/10.1021/acsomega.3c06110

Author Contributions

‖P.G. and R.R. contributed equally.

Notes

The authors declare no competing financial interest.

■ ACKNOWLEDGMENTS

The authors thank the bioinstrumentation facility, Indian Institutes of Science Education and Research Bhopal, for assistance with the flow cytometry experiments.

■ REFERENCES

(1) Jemal, A.; Siegel, R.; Xu, J.; Ward, E. Cancer Statistics, 2010. *Ca-Cancer J. Clin.* **2010**, *60* (5), 277−300.

(2) Lathia, J. D.; Mack, S. C.; Mulkearns-Hubert, E. E.; Valentim, C. L. L.; Rich, J. N. Cancer Stem Cells in Glioblastoma. *Genes Dev.* **2015**, *29* (12), 1203−1217.

(3) Alexander, B. M.; Cloughesy, T. F. Adult Glioblastoma. *J. Clin. Oncol.* **2017**, *35* (21), 2402−2409.

(4) Westphal, M.; Maire, C. L.; Lamszus, K. EGFR as a Target for Glioblastoma Treatment: An Unfulfilled Promise. *CNS Drugs* **2017**, *31* (9), 723−735.

(5) Cohen, P.; Cross, D.; Jänne, P. A. Kinase Drug Discovery 20 Years after Imatinib: Progress and Future Directions. *Nat. Rev. Drug Discovery* **2021**, *20* (7), 551−569.

(6) Jimenez-Pascual, A.; A Siebzehnrubl, F. Fibroblast Growth Factor Receptor Functions in Glioblastoma. *Cells* **2019**, *8* (7), 715.

(7) Anwar, S.; Shamsi, A.; Shahbaaz, M.; Queen, A.; Khan, P.; Hasan, G. M.; Islam, A.; Alajmi, M. F.; Hussain, A.; Ahmad, F.; Hassan, M. I. Rosmarinic Acid Exhibits Anticancer Effects via MARK4 Inhibition. *Sci. Rep.* **2020**, *10* (1), 10300.

(8) Singh, S.; Sadhukhan, S.; Sonawane, A. 20 Years since the Approval of First EGFR-TKI, Gefitinib: Insight and Foresight. *Biochim. Biophys. Acta, Rev. Cancer* **2023**, *1878* (6), 188967.

(9) Cohen, M. H.; Williams, G. A.; Sridhara, R.; Chen, G.; Pazdur, R. FDA Drug Approval Summary: Gefitinib (ZD1839) (Iressa) Tablets. *Oncologist* **2003**, *8* (4), 303−306.

(10) Dungo, R. T.; Keating, G. M. Afatinib: First Global Approval. *Drugs* **2013**, *73*, 1503−1515.

(11) Koch, A. L.; Vellanki, P. J.; Drezner, N.; Li, X.; Mishra-Kalyani, P. S.; Shen, Y. L.; Xia, H.; Li, Y.; Liu, J.; Zirkelbach, J. F.; et al. FDA Approval Summary: Osimertinib for Adjuvant Treatment of Surgically Resected Non-Small Cell Lung Cancer, a Collaborative Project Orbis Review. *Clin. Cancer Res.* **2021**, *27* (24), 6638−6643.

(12) Ryan, Q.; Ibrahim, A.; Cohen, M. H.; Johnson, J.; Ko, C.; Sridhara, R.; Justice, R.; Pazdur, R. FDA Drug Approval Summary: Lapatinib in Combination with Capecitabine for Previously Treated Metastatic Breast Cancer That Overexpresses HER-2. *Oncologist* **2008**, *13* (10), 1114−1119.

(13) Fogli, S.; Porta, C.; Del Re, M.; Crucitta, S.; Gianfilippo, G.; Danesi, R.; Rini, B. I.; Schmidinger, M. Optimizing Treatment of Renal Cell Carcinoma with VEGFR-TKIs: A Comparison of Clinical Pharmacology and Drug-Drug Interactions of Anti-Angiogenic Drugs. *Cancer Treat. Rev.* **2020**, *84*, 101966.

(14) Pant, S.; Schuler, M.; Iyer, G.; Witt, O.; Doi, T.; Qin, S.; Tabernero, J.; Reardon, D. A.; Massard, C.; Minchom, A.; Lugowska, I.; Carranza, O.; Arnold, D.; Gutierrez, M.; Winter, H.; Stuyckens, K.; Crow, L.; Najmi, S.; Hammond, C.; Thomas, S.; Santiago-Walker, A.; Triantos, S.; Sweiti, H.; Loriot, Y.; et al. Erdafitinib in patients with advanced solid tumours with FGFR alterations (RAGNAR): an international, single-arm, phase 2 study. *Lancet Oncol.* **2023**, *24* (8), 925−935.

(15) Sharma, S. V.; Gajowniczek, P.; Way, I. P.; Lee, D. Y.; Jiang, J.; Yuza, Y.; Classon, M.; Haber, D. A.; Settleman, J. A Common Signaling Cascade May Underlie "Addiction" to the Src, BCR-ABL, and EGF Receptor Oncogenes. *Cancer Cell* **2006**, *10* (5), 425−435.

(16) Frustaci, A. M.; Deodato, M.; Zamprogna, G.; Cairoli, R.; Montillo, M.; Tedeschi, A. Next Generation BTK Inhibitors in CLL: Evolving Challenges and New Opportunities. *Cancers* **2023**, *15* (5), 1504.

(17) Klein, M. E.; Kovatcheva, M.; Davis, L. E.; Tap, W. D.; Koff, A. CDK4/6 Inhibitors: The Mechanism of Action May Not Be as Simple as Once Thought. *Cancer Cell* **2018**, *34* (1), 9−20.

(18) E Taylor, T.; B Furnari, F.; K Cavenee, W. Targeting EGFR for Treatment of Glioblastoma: Molecular Basis to Overcome Resistance. *Curr. Cancer Drug Targets* **2012**, *12* (3), 197−209.

(19) Singh, M.; Jadhav, H. R. Targeting Non-Small Cell Lung Cancer with Small-Molecule EGFR Tyrosine Kinase Inhibitors. *Drug Discovery Today* **2018**, *23* (3), 745−753.

(20) Henson, E. S.; Gibson, S. B. Surviving Cell Death through Epidermal Growth Factor (EGF) Signal Transduction Pathways: Implications for Cancer Therapy. *Cell Signal* **2006**, *18* (12), 2089−2097.

(21) Ray, M.; Salgia, R.; Vokes, E. E. The Role of EGFR Inhibition in the Treatment of Non-Small Cell Lung Cancer. *Oncologist* **2009**, *14* (11), 1116−1130.

(22) Tan, C.-S.; Kumarakulasinghe, N. B.; Huang, Y.-Q.; Ang, Y. L. E.; Choo, J. R.-E.; Goh, B.-C.; Soo, R. A. Third Generation EGFR TKIs: Current Data and Future Directions. *Mol. Cancer* **2018**, *17* (1), 29.

(23) Passaro, A.; Jänne, P. A.; Mok, T.; Peters, S. Overcoming Therapy Resistance in EGFR-Mutant Lung Cancer. *Nat. Cancer* **2021**, *2* (4), 377−391.

(24) Du, X.; Yang, B.; An, Q.; Assaraf, Y. G.; Cao, X.; Xia, J. Acquired Resistance to Third-Generation EGFR-TKIs and Emerging Next-Generation EGFR Inhibitors. *Innovation* **2021**, *2* (2), 100103.

(25) Cui, J.; Hu, Y.-F.; Feng, X.-M.; Tian, T.; Guo, Y.-H.; Ma, J.-W.; Nan, K.-J.; Zhang, H.-Y. EGFR Inhibitors and Autophagy in Cancer Treatment. *Tumour Biol.* **2014**, *35* (12), 11701−11709.

(26) Chen, Y.; Henson, E. S.; Xiao, W.; Huang, D.; McMillan-Ward, E. M.; Israels, S. J.; Gibson, S. B. Tyrosine Kinase Receptor EGFR Regulates the Switch in Cancer Cells between Cell Survival and Cell Death Induced by Autophagy in Hypoxia. *Autophagy* **2016**, *12* (6), 1029−1046.

(27) Duffy, A.; Le, J.; Sausville, E.; Emadi, A. Autophagy Modulation: A Target for Cancer Treatment Development. *Cancer Chemother. Pharmacol.* **2015**, *75*, 439−447.

(28) Ho, C. J.; Gorski, S. M. Molecular Mechanisms Underlying Autophagy-Mediated Treatment Resistance in Cancer. *Cancers* **2019**, *11* (11), 1775.

(29) Peng, Y.; Wang, Y.; Zhou, C.; Mei, W.; Zeng, C. PI3K/Akt/mTOR Pathway and Its Role in Cancer Therapeutics: Are We Making Headway? *Front. Oncol.* **2022**, *12*, 819128.

(30) Xu, Z.; Han, X.; Ou, D.; Liu, T.; Li, Z.; Jiang, G.; Liu, J.; Zhang, J. Targeting PI3K/AKT/mTOR-Mediated Autophagy for Tumor Therapy. *Appl. Microbiol. Biotechnol.* **2020**, *104* (2), 575−587.
(31) Sahadevan, R.; Singh, S.; Binoy, A.; Sadhukhan, S. Chemico-Biological Aspects of (-)-Epigallocatechin-3-Gallate (EGCG) to Improve Its Stability, Bioavailability and Membrane Permeability: Current Status and Future Prospects. *Crit. Rev. Food Sci. Nutr.* **2022**, 1−30.
(32) Majrashi, T. A.; Alshehri, S. A.; Alsayari, A.; Muhsinah, A. B.; Alrouji, M.; Alshahrani, A. M.; Shamsi, A.; Atiya, A. Insight into the Biological Roles and Mechanisms of Phytochemicals in Different Types of Cancer: Targeting Cancer Therapeutics. *Nutrients* **2023**, *15* (7), 1704.
(33) Sahadevan, R.; Binoy, A.; Vechalapu, S. K.; Nanjan, P.; Sadhukhan, S. In Situ Global Proteomics Profiling of EGCG Targets Using a Cell-Permeable and Click-Able Bioorthogonal Probe. *Int. J. Biol. Macromol.* **2023**, *237*, 123991.
(34) Bakun, P.; Mlynarczyk, D. T.; Koczorowski, T.; Cerbin-Koczorowska, M.; Piwowarczyk, L.; Kolasiński, E.; Stawny, M.; Kuźmińska, J.; Jelińska, A.; Goslinski, T. Tea-Break with Epigallocatechin Gallate Derivatives—Powerful Polyphenols of Great Potential for Medicine. *Eur. J. Med. Chem.* **2023**, *261*, 115820.
(35) Chakrawarti, L.; Agrawal, R.; Dang, S.; Gupta, S.; Gabrani, R. Therapeutic Effects of EGCG: A Patent Review. *Expert Opin. Ther. Pat.* **2016**, *26* (8), 907−916.
(36) Krupkova, O.; Ferguson, S. J.; Wuertz-Kozak, K. Stability of (-)-Epigallocatechin Gallate and Its Activity in Liquid Formulations and Delivery Systems. *J. Nutr. Biochem.* **2016**, *37*, 1−12.
(37) Gan, R.-Y.; Li, H.-B.; Sui, Z.-Q.; Corke, H. Absorption, Metabolism, Anti-Cancer Effect and Molecular Targets of Epigallocatechin Gallate (EGCG): An Updated Review. *Crit. Rev. Food Sci. Nutr.* **2018**, *58* (6), 924−941.
(38) Zhang, S.; Mao, B.; Cui, S.; Zhang, Q.; Zhao, J.; Tang, X.; Chen, W. Absorption, Metabolism, Bioactivity, and Biotransformation of Epigallocatechin Gallate. *Crit. Rev. Food Sci. Nutr.* **2023**, 1−21.
(39) Minnelli, C.; Galeazzi, R.; Laudadio, E.; Amici, A.; Rusciano, D.; Armeni, T.; Cantarini, M.; Stipa, P.; Mobbili, G. Monoalkylated Epigallocatechin-3-Gallate (C18-EGCG) as Novel Lipophilic EGCG Derivative: Characterization and Antioxidant Evaluation. *Antioxidants* **2020**, *9* (3), 208.
(40) Singh, S.; Sahadevan, R.; Roy, R.; Biswas, M.; Ghosh, P.; Kar, P.; Sonawane, A.; Sadhukhan, S. Structure-Based Design and Synthesis of a Novel Long-Chain 4″-Alkyl Ether Derivative of EGCG as Potent EGFR Inhibitor: In Vitro and in Silico Studies. *RSC Adv.* **2022**, *12* (28), 17821−17836.
(41) Hu, H.; Zhang, X.-W.; Li, L.; Hu, M.-N.; Hu, W.-Q.; Zhang, J.-Y.; Miao, X.-K.; Yang, W.-L.; Mou, L.-Y. Inhibition of Autophagy by YC-1 Promotes Gefitinib Induced Apoptosis by Targeting FOXO1 in Gefitinib-Resistant NSCLC Cells. *Eur. J. Pharmacol.* **2021**, *908*, 174346.
(42) Pragti; Kundu, B. K.; Singh, S.; Carlton Ranjith, W. A.; Sarkar, S.; Sonawane, A.; Mukhopadhyay, S. Chitosan-Biotin-Conjugated pH-Responsive Ru(II) Glucose Nanogel: A Dual Pathway of Targeting Cancer Cells and Self-Drug Delivery. *ACS Appl. Mater. Interfaces* **2023**, *15*, 43345−43358.
(43) Pragti; Nayek, S.; Singh, S.; Sonawane, A.; Grabchev, I.; Ganguly, R.; Mukhopadhyay, S. Studies on Anticancer Properties with Varying Co-Ligands in a Ru(II) Arene Benzimidazole System. *Dalton Trans.* **2023**, *52* (21), 7104−7118.
(44) Friesner, R. A.; Banks, J. L.; Murphy, R. B.; Halgren, T. A.; Klicic, J. J.; Mainz, D. T.; Repasky, M. P.; Knoll, E. H.; Shelley, M.; Perry, J. K.; Shaw, D. E.; Francis, P.; Shenkin, P. S. Glide: A New Approach for Rapid, Accurate Docking and Scoring. 1. Method and Assessment of Docking Accuracy. *J. Med. Chem.* **2004**, *47* (7), 1739−1749.
(45) Friesner, R. A.; Murphy, R. B.; Repasky, M. P.; Frye, L. L.; Greenwood, J. R.; Halgren, T. A.; Sanschagrin, P. C.; Mainz, D. T. Extra Precision Glide: Docking and Scoring Incorporating a Model of Hydrophobic Enclosure for Protein-Ligand Complexes. *J. Med. Chem.* **2006**, *49* (21), 6177−6196.
(46) Webb, B.; Sali, A. Comparative Protein Structure Modeling Using MODELLER. *Curr. Protoc. Bioinf.* **2014**, *47* (1), 5.
(47) Harder, E.; Damm, W.; Maple, J.; Wu, C.; Reboul, M.; Xiang, J. Y.; Wang, L.; Lupyan, D.; Dahlgren, M. K.; Knight, J. L.; Kaus, J. W.; Cerutti, D. S.; Krilov, G.; Jorgensen, W. L.; Abel, R.; Friesner, R. A. OPLS3: A Force Field Providing Broad Coverage of Drug-like Small Molecules and Proteins. *J. Chem. Theory Comput.* **2016**, *12* (1), 281−296.
(48) Maier, J. A.; Martinez, C.; Kasavajhala, K.; Wickstrom, L.; Hauser, K. E.; Simmerling, C. ff14SB: Improving the Accuracy of Protein Side Chain and Backbone Parameters from ff99SB. *J. Chem. Theory Comput.* **2015**, *11* (8), 3696−3713.
(49) Wang, J.; Wolf, R. M.; Caldwell, J. W.; Kollman, P. A.; Case, D. A. Development and Testing of a General Amber Force Field. *J. Comput. Chem.* **2004**, *25* (9), 1157−1174.
(50) Wang, B.; Merz, K. M. A Fast QM/MM (Quantum Mechanical/Molecular Mechanical) Approach to Calculate Nuclear Magnetic Resonance Chemical Shifts for Macromolecules. *J. Chem. Theory Comput.* **2006**, *2* (1), 209−215.
(51) Jorgensen, W. L.; Chandrasekhar, J.; Madura, J. D.; Impey, R. W.; Klein, M. L. Comparison of Simple Potential Functions for Simulating Liquid Water. *J. Chem. Phys.* **1983**, *79* (2), 926−935.
(52) Kräutler, V.; Van Gunsteren, W. F.; Hünenberger, P. H. A Fast SHAKE Algorithm to Solve Distance Constraint Equations for Small Molecules in Molecular Dynamics Simulations. *J. Comput. Chem.* **2001**, *22* (5), 501−508.
(53) Darden, T.; York, D.; Pedersen, L. Particle mesh Ewald: An $N\cdot\log(N)$ method for Ewald sums in large systems. *J. Chem. Phys.* **1993**, *98* (12), 10089−10092.
(54) Allen, M. P.; Tildesley, D. J. *Computer Simulation of Liquids*, 2nd; Oxford University PressOxford, 2017.
(55) Berendsen, H. J. C.; Postma, J. P. M.; Van Gunsteren, W. F.; DiNola, A.; Haak, J. R. Molecular Dynamics with Coupling to an External Bath. *J. Chem. Phys.* **1984**, *81* (8), 3684−3690.
(56) Roy, R.; Ghosh, B.; Kar, P. Investigating Conformational Dynamics of Lewis Y Oligosaccharides and Elucidating Blood Group Dependency of Cholera Using Molecular Dynamics. *ACS Omega* **2020**, *5* (8), 3932−3942.
(57) Roy, R.; Mishra, A.; Poddar, S.; Nayak, D.; Kar, P. Investigating the Mechanism of Recognition and Structural Dynamics of Nucleoprotein-RNA Complex from Peste Des Petits Ruminants Virus via Gaussian Accelerated Molecular Dynamics Simulations. *J. Biomol. Struct. Dyn.* **2022**, *40* (5), 2302−2315.
(58) Thurakkal, L.; Singh, S.; Roy, R.; Kar, P.; Sadhukhan, S.; Porel, M. An In-Silico Study on Selected Organosulfur Compounds as Potential Drugs for SARS-CoV-2 Infection via Binding Multiple Drug Targets. *Chem. Phys. Lett.* **2021**, *763*, 138193.
(59) Singh, S.; Sk, M. F.; Sonawane, A.; Kar, P.; Sadhukhan, S. Plant-Derived Natural Polyphenols as Potential Antiviral Drugs against SARS-CoV-2 via RNA-Dependent RNA Polymerase (RdRp) Inhibition: An in-Silico Analysis. *J. Biomol. Struct. Dyn.* **2021**, *39* (16), 6249−6264.
(60) Roe, D. R.; Cheatham, T. E. PTRAJ and CPPTRAJ: Software for Processing and Analysis of Molecular Dynamics Trajectory Data. *J. Chem. Theory Comput.* **2013**, *9* (7), 3084−3095.
(61) Shamsi, A.; Shahwan, M.; Khan, M. S.; Husain, F. M.; Alhumaydhi, F. A.; Aljohani, A. S. M.; Rehman, M. T.; Hassan, M. I.; Islam, A. Elucidating the Interaction of Human Ferritin with Quercetin and Naringenin: Implication of Natural Products in Neurodegenerative Diseases: Molecular Docking and Dynamics Simulation Insight. *ACS Omega* **2021**, *6* (11), 7922−7930.
(62) Roy, R.; Poddar, S.; Sk, M. F.; Kar, P. Conformational Preferences of Triantennary and Tetraantennary Hybrid N-Glycans in Aqueous Solution: Insights from 20 Ms Long Atomistic Molecular Dynamic Simulations. *J. Biomol. Struct. Dyn.* **2023**, *41* (8), 3305−3320.
(63) Roy, R.; Sk, M. F.; Tanwar, O.; Kar, P. Computational Studies Indicated the Effectiveness of Human Metabolites against SARS-Cov-2 Main Protease. *Mol. Diversity* **2023**, *27* (4), 1587−1602.

https://doi.org/10.1021/acsomega.3c06110
ACS Omega 2024, 9, 2286−2301

(64) Kollman, P. A.; Massova, I.; Reyes, C.; Kuhn, B.; Huo, S.; Chong, L.; Lee, M.; Lee, T.; Duan, Y.; Wang, W.; Donini, O.; Cieplak, P.; Srinivasan, J.; Case, D. A.; Cheatham, T. E. Calculating Structures and Free Energies of Complex Molecules: Combining Molecular Mechanics and Continuum Models. *Acc. Chem. Res.* **2000**, *33* (12), 889−897.
(65) Uribe, M. L.; Marrocco, I.; Yarden, Y. EGFR in Cancer: Signaling Mechanisms, Drugs, and Acquired Resistance. *Cancers* **2021**, *13* (11), 2748.
(66) Wei, Y.; Zou, Z.; Becker, N.; Anderson, M.; Sumpter, R.; Xiao, G.; Kinch, L.; Koduru, P.; Christudass, C. S.; Veltri, R. W.; Grishin, N. V.; Peyton, M.; Minna, J.; Bhagat, G.; Levine, B. EGFR-Mediated Beclin 1 Phosphorylation in Autophagy Suppression, Tumor Progression, and Tumor Chemoresistance. *Cell* **2013**, *154* (6), 1269−1284.
(67) Wu, M.; Zhang, P. EGFR-Mediated Autophagy in Tumourigenesis and Therapeutic Resistance. *Cancer Lett.* **2020**, *469*, 207−216.
(68) Liu, X.; Suo, H.; Zhou, S.; Hou, Z.; Bu, M.; Liu, X.; Xu, W. Afatinib Induces Pro-Survival Autophagy and Increases Sensitivity to Apoptosis in Stem-like HNSCC Cells. *Cell Death Dis.* **2021**, *12* (8), 728.
(69) Kwon, Y.; Kim, M.; Jung, H. S.; Kim, Y.; Jeoung, D. Targeting Autophagy for Overcoming Resistance to Anti-EGFR Treatments. *Cancers* **2019**, *11* (9), 1374.
(70) Tanida, I.; Ueno, T.; Kominami, E. LC3 and Autophagy. *Methods Mol. Biol.* **2008**, *445*, 77−88.
(71) Chang, Z.; Shi, G.; Jin, J.; Guo, H.; Guo, X.; Luo, F.; Song, Y.; Jia, X. Dual PI3K/mTOR Inhibitor NVP-BEZ235-Induced Apoptosis of Hepatocellular Carcinoma Cell Lines Is Enhanced by Inhibitors of Autophagy. *Int. J. Mol. Med.* **2013**, *31* (6), 1449−1456.
(72) Lim, Z.-F.; Ma, P. C. Emerging Insights of Tumor Heterogeneity and Drug Resistance Mechanisms in Lung Cancer Targeted Therapy. *J. Hematol. Oncol.* **2019**, *12* (1), 134.
(73) Das, C. K.; Mandal, M.; Kögel, D. Pro-Survival Autophagy and Cancer Cell Resistance to Therapy. *Cancer Metastasis Rev.* **2018**, *37* (4), 749−766.
(74) Leboffe, L.; Di Masi, A.; Polticelli, F.; Trezza, V.; Ascenzi, P. Structural Basis of Drug Recognition by Human Serum Albumin. *Curr. Med. Chem.* **2020**, *27* (30), 4907−4931.
(75) Mali, G.; Maji, S.; Chavan, K. A.; Shukla, M.; Kumar, M.; Bhattacharyya, S.; Erande, R. D. Effective Synthesis and Biological Evaluation of Functionalized 2,3-Dihydrofuro[3,2-c]Coumarins via an Imidazole-Catalyzed Green Multicomponent Approach. *ACS Omega* **2022**, *7* (40), 36028−36036.
(76) Molaei, P.; Mahaki, H.; Manoochehri, H.; Tanzadehpanah, H. Binding Sites of Anticancer Drugs on Human Serum Albumin (HSA): AReview. *Protein Pept. Lett.* **2022**, *29* (8), 651−675.
(77) Kanwal, U.; Irfan Bukhari, N.; Ovais, M.; Abass, N.; Hussain, K.; Raza, A. Advances in Nano-Delivery Systems for Doxorubicin: An Updated Insight. *J. Drug Targeting* **2018**, *26* (4), 296−310.
(78) Das, M.; Mukherjee, S.; Brandao, P.; Seth, S. K.; Giri, S.; Mati, S. S.; Samanta, B. C.; Laha, S.; Maity, T. Active Bromoaniline-Aldehyde Conjugate Systems and Their Complexes as Versatile Sensors of Multiple Cations with Logic Formulation and Efficient DNA/HSA-Binding Efficacy: Combined Experimental and Theoretical Approach. *ACS Omega* **2021**, *6* (5), 3659−3674.
(79) Strugała, P.; Dudra, A.; Gabrielska, J. Interaction between Mimic Lipid Membranes and Acylated and Nonacylated Cyanidin and Its Bioactivity. *J. Agric. Food Chem.* **2016**, *64* (39), 7414−7422.
(80) Taverna, M.; Marie, A.-L.; Mira, J.-P.; Guidet, B. Specific Antioxidant Properties of Human Serum Albumin. *Ann. Intensive Care* **2013**, *3* (1), 4.
(81) Levy, J. M. M.; Towers, C. G.; Thorburn, A. Targeting Autophagy in Cancer. *Nat. Rev. Cancer* **2017**, *17* (9), 528−542.
(82) Lin, C.-J.; Lee, C.-C.; Shih, Y.-L.; Lin, C.-H.; Wang, S.-H.; Chen, T.-H.; Shih, C.-M. Inhibition of Mitochondria- and Endoplasmic Reticulum Stress-Mediated Autophagy Augments Temozolomide-Induced Apoptosis in Glioma Cells. *PLoS One* **2012**, *7* (6), No. e38706.
(83) Zhao, Z.-Q.; Yu, Z.-Y.; Li, J.; Ouyang, X.-N. Gefitinib Induces Lung Cancer Cell Autophagy and Apoptosis via Blockade of the PI3K/AKT/mTOR Pathway. *Oncol. Lett.* **2016**, *12* (1), 63−68.
(84) Li, Y.-Y.; Lam, S.-K.; Mak, J. C.-W.; Zheng, C.-Y.; Ho, J. C.-M. Erlotinib-Induced Autophagy in Epidermal Growth Factor Receptor Mutated Non-Small Cell Lung Cancer. *Lung Cancer* **2013**, *81* (3), 354−361.
(85) Li, L.; Wang, Y.; Jiao, L.; Lin, C.; Lu, C.; Zhang, K.; Hu, C.; Ye, J.; Zhang, D.; Wu, H.; et al. Protective Autophagy Decreases Osimertinib Cytotoxicity through Regulation of Stem Cell-like Properties in Lung Cancer. *Cancer Lett.* **2019**, *452*, 191−202.
(86) Sameiyan, E.; Hayes, A. W.; Karimi, G. The Effect of Medicinal Plants on Multiple Drug Resistance through Autophagy: A Review of in Vitro Studies. *Eur. J. Pharmacol.* **2019**, *852*, 244−253.
(87) Hashemzaei, M.; Entezari Heravi, R.; Rezaee, R.; Roohbakhsh, A.; Karimi, G. Regulation of Autophagy by Some Natural Products as a Potential Therapeutic Strategy for Cardiovascular Disorders. *Eur. J. Pharmacol.* **2017**, *802*, 44−51.
(88) Hu, X.; Shi, S.; Wang, H.; Yu, X.; Wang, Q.; Jiang, S.; Ju, D.; Ye, L.; Feng, M. Blocking Autophagy Improves the Anti-Tumor Activity of Afatinib in Lung Adenocarcinoma with Activating EGFR Mutations in vitro and in vivo. *Sci. Rep.* **2017**, *7* (1), 4559.

https://doi.org/10.1021/acsomega.3c06110
ACS Omega 2024, 9, 2286−2301